THE ASTROPHYSICAL JOURNAL, 494:150–174, 1998 February 10

STARBURST GALAXIES. III. PROPERTIES OF A RADIO-SELECTED SAMPLE[1]

DENISE A. SMITH,[2,3] TERRY HERTER,[2] AND MARTHA P. HAYNES[2]
Center for Radiophysics and Space Research, Space Sciences Building, Cornell University, Ithaca, NY 14853;
dsmith@stsci.edu, herter@astrosun.tn.cornell.edu, haynes@astrosun.tn.cornell.edu
Received 1996 July 9; accepted 1997 September 22

ABSTRACT

We have analyzed the properties of the 20 most radio-luminous UGC starburst galaxies from Condon, Frayer, & Broderick. Near-infrared images, spectra, and optical rotation curves were presented in Smith et al. In this paper, we use these data and published radio data to assess the stellar populations, dust contents, ionizing conditions, and dynamics of the starbursts.

Certain properties of the star formation occurring in these galaxies differ from those observed locally. The infrared excesses (IREs) are lower than and span a narrower range of values than those of Galactic H II regions. The starbursts appear to produce a higher proportion of ionizing photons than most Galactic H II regions. Consequently, the initial mass functions (IMFs) of the starbursts may be more strongly biased toward high-mass star formation. The starbursts may also contain fewer old H II regions than the Milky Way. Furthermore, the starburst IRE is likely to be influenced by the presence of large reservoirs of gas that absorb a larger fraction of the Lyman continuum photons. The OB stellar and far-infrared luminosities imply that the upper mass range of the starburst IMF ($M > 10\ M_{\odot}$) is characterized by a slope of 2.7 ± 0.2. The starburst IMF thus bears a strong similarity to that observed in Magellanic OB associations. Optical line ratios indicate that a range of excitation conditions are present.

We conclude that the near-infrared light from many of the starbursts is dominated by a heavily obscured mixture of emission from evolved red stars and young blue stars with small contributions ($\approx 5\%$) from thermal gas and hot dust, under the assumptions that a Galactic or SMC extinction law can be applied to these systems and that the true reddening curve follows one of the models currently existing in the literature. In some cases, larger amounts of emission from blue stars or hot dust may be required to explain the observed near-infrared colors. The amount of dust emission exceeds that predicted from comparisons with Galactic H II regions. The near-infrared colors of some of the systems may also be influenced by the presence of a low-luminosity active galactic nucleus (AGN). Emission from blue stars and hot dust, if present, dilutes the observed CO index. The activity in the redder, more luminous systems is strongly peaked.

The galaxies hosting the starbursts exhibit a wide range of morphological and star-forming properties. While all of the host galaxies are interacting systems, the nuclear separations of the interacting nuclei range from <1 kpc to >1 Mpc. The dynamical behavior ranges from relaxed to strongly perturbed. The off-nuclear regions of the galaxies are sites of active star formation and are characterized by a range of excitation conditions. Spatially extended LINER emission is consistent with shock excitation produced by superwinds or galaxy-galaxy collisions. Violent star formation activity occurs over a larger physical scale in the most active starbursts. Systems containing mergers and widely separated nuclei possess similar colors and luminosities. The burst properties are most likely regulated by the internal structures of the interacting galaxies and not the separations of the interacting galaxies.

Subject headings: galaxies: interactions — galaxies: starburst — infrared: galaxies

1. INTRODUCTION

The phrase "starburst galaxy" has come into widespread usage to describe a class of galaxies whose spectral properties are best explained in terms of a population of hot young stars formed over a short period of time. This rapid star formation activity may be triggered by galaxy-galaxy interactions and mergers, stellar bars, and/or active galactic nuclei (AGNs). The fact that starbursts are present in many galaxies suggests that all galaxies may undergo a burst of intense star formation at some point in their evolution and raises the issue of whether or not the first generation of star formation occurred via this process (Soifer, Houck, & Neugebauer 1987). Recent observations with the *Hubble Space Telescope* indicate that galaxy-galaxy interactions and starbursts may indeed play a fundamental role in galaxy evolution at earlier epochs (Dressler et al. 1994; Couch et al. 1994; Driver, Windhorst, & Griffiths 1995). As the quest for high-redshift galaxies undergoing their first episode of star formation continues, several fundamental issues regarding the starburst phenomenon remain unanswered. For example, several studies suggest that M82, the "prototypical" starburst galaxy, is biased against the formation of low-mass stars (Rieke et al. 1980, 1993; Doane & Mathews 1993). The frequency with which such bias occurs is not known, however. The degree of similarity between the star formation occurring in starbursts and that observed locally thus remains a subject of debate.

Observations of nearby starburst galaxies provide a unique opportunity to obtain a detailed understanding of

[1] Observations at the Palomar Observatory were made as part of a continuing collaborative agreement between the California Institute of Technology and Cornell University.

[2] Visiting Astronomer, Kitt Peak National Observatory, National Optical Astronomy Observatories, operated by AURA, Inc. under a cooperative agreement with the National Science Foundation.

[3] Current address: Space Telescope Science Institute, 3700 San Martin Drive, Baltimore, MD 21218.

this enigmatic mode of star formation activity. This is the third paper in a series devoted to the study of the 20 most radio-luminous UGC starburst galaxies from the survey of Condon, Frayer, & Broderick (1991b; hereafter CFB91). These authors classify the dominant energy sources in 347 UGC galaxies with 5 GHz fluxes in excess of 25 mJy as starbursts or AGNs on the basis of the ratio of their radio and far-infrared fluxes, their radio morphologies, and/or their far-infrared spectral indices. Since the radio emission from a starburst arises from H II regions and from supernovae and is essentially unaffected by extinction, the starbursts identified by CFB91 form a sample of relatively nearby northern hemisphere starburst systems that is independent of the dust content of the host galaxy, in contrast to samples based upon ultraviolet, optical, or far-infrared fluxes. The application of a luminosity criterion ensures that our subsample of 20 galaxies is based upon an intrinsic starburst property. We note that the well-known correlation between radio and far-infrared fluxes implies that these galaxies are also luminous in the far-infrared (Helou, Soifer, & Rowan-Robinson 1985; Condon, Anderson, & Helou 1991a). However, our sample differs from existing samples of infrared-luminous galaxies (ILGs) in that most studies of ILGs include both starbursts and AGNs. The radio-luminous starbursts also have a nearby optical counterpart, namely a UGC galaxy, whereas the most infrared-luminous sources are not necessarily nearby sources and do not necessarily possess an obvious optical counterpart. Our sample also differs from other starburst samples (see, e.g., Balzano 1983; Joseph et al. 1984; Devereux 1989) in that morphological criteria have not been applied during the process of sample selection. Consequently, properties such as the spatial extent of the burst and the morphology of the host galaxy are free parameters in this study. Table 1 lists selected properties of the sample and summarizes the nomenclature of sources with multiple components. Three "normal" spiral galaxies serve as comparison sources. The reader is referred to Smith et al. (1996) for additional information regarding the individual galaxies comprising the sample.

Our study uses near-infrared and optical observations, published radio data, and stellar population models to characterize the properties of these nearby starbursts and to assess the degree of similarity between star formation occurring in starbursts and that observed locally. Smith et al. (1995; hereafter Paper I) outlines our goals and techniques and presents the results of near-infrared broadband imaging and K-band spectroscopy of UGC 8387, the first galaxy in the sample for which a complete data set was obtained. Star formation in this merging galaxy differs from that occurring in "normal" galaxies in that a significant portion of the 2 μm continuum emission is produced by hot dust. The initial mass function (IMF) for UGC 8387 appears to be biased toward the formation of high-mass stars. A description of the entire sample and data set, including J, H, and K broadband images, K-band spectra, and optical rotation curves, is given in Smith et al. (1996; hereafter Paper II). We find that all 20 galaxies are either mergers, interacting pairs, or members of groups or clusters. These facts suggest that the starbursts were most likely triggered by interactions with other galaxies. Paper II also presents the J, H, and K band fluxes, $H-K$ and $J-H$ colors, and CO indices derived from these data. The near-infrared colors of the starburst nuclei are found to be redder than those of "normal" galaxies. The data also indicate that many of the galaxies possess strong CO absorption features. Where sufficient data exist, Brγ fluxes, optical depths, and dynamical masses are also calculated in Paper II. An average optical depth of $A_V \sim 25$ is derived from the Brγ and the radio fluxes emitted by five of the galaxies for the case of an overlying dust screen; these starbursts are heavily obscured. Optical rotation curves imply an average dynamical mass of $\sim 10^9\ M_\odot$.

In this paper, we use the measurements from Paper II and published radio data to characterize the starburst phenomenon. Star formation properties are derived for the sample galaxies and compared to those of the "prototypical" starburst galaxy M82 and the Milky Way. The dynamics of the systems, as well as correlations between the properties of the nuclear and off-nuclear regions of the starbursts, trace the evolution of starburst activity.

TABLE 1

THE STARBURST GALAXY SAMPLE

Galaxy	D[a] (Mpc)	$L_{4.85}$[b] (W Hz^{-1})	L_{IR}[c] ($L_\odot$)	Status
UGC 1315	129.40	22.70	11.50	Interacting?
UGC 1655	71.65	22.46	11.22	Cluster member
UGC 2238	86.44	22.48	11.19	Merger
UGC 2608	93.89	22.67	11.20	Cluster member
UGC 3334	52.47	22.30	10.85	Group member
UGC 3351	64.00	22.35	11.19	Pair
UGC 3608[d]	85.85	22.34	11.12	Interacting
UGC 4509	73.44	22.58	11.44	Merger
UGC 4756[d]	197.99	23.10	11.61	Interacting
UGC 5101	160.00	23.38	11.86	Merger
UGC 6471/2[d]	41.53	22.79	11.58	Interacting
UGC 8335[d]	124.17	22.70	11.57	Interacting
UGC 8387	91.92	22.67	11.46	Merger
UGC 8696	149.07	23.44	12.04	Merger
UGC 9618[d]	135.55	22.92	11.52	Pair
UGC 9913	72.85	23.11	12.06	Merger
UGC 10182[d]	60.00	22.24	10.74	Interacting
UGC 10647	74.67	22.48	11.19	Pair
UGC 12332	64.69	22.48	11.37	Pair
UGC 12815	56.75	22.36	11.19	Group member
UGC 1248[e]	62.32	...	9.86	Cluster member
UGC 2085[e]	90.41	...	9.46	Cluster member
UGC 8220[e]	95.08	...	10.09	Cluster member
M82	3.60	21.82	10.54	Interacting

NOTE.—A value of $H_0 = 75$ km s^{-1} Mpc^{-1} is assumed throughout this paper.

[a] Distance derived from the heliocentric radial velocity listed in the AGC, a private database maintained by R. Giovanelli and M. P. Haynes.

[b] Logarithm of the 4.85 GHz luminosity (W Hz^{-1}) calculated from the 4.85 GHz fluxes quoted by CFB91.

[c] Logarithm of the color-corrected far-infrared luminosity between 1 and 500 μm ($L_\odot$) derived from the far-infrared flux (IR = 1.26 $\times 10^{-14}$ [2.58f_ν(60 μm) + f_ν(100 μm)] W m^{-2}) (Helou et al. 1988), a grain emissivity of λ^{-1}, and Appendix B of Lonsdale et al. (1985). The quantities f_ν(60 μm) and f_ν(100 μm) are the 60 and 100 μm *IRAS* flux densities in janskys.

[d] Multiple nuclei. UGC 3608: UGC 3608N = companion = northern nucleus, UGC 3608S = starburst nucleus = southern nucleus. UGC 4756: UGC 4756A = southeastern source, UGC 4756B = central source, UGC 4756C = northwestern source. UGC 6471/2: UGC 6471 = IC 694 = NGC 3690A, UGC 6472B = NGC 3690B, UGC 6472C = NGC 3690C. UGC 8335: UGC 8335E = starburst nucleus = eastern source, UGC 8335W = companion = western source. UGC 9618: UGC 9618N = starburst nucleus = northern source, UGC 9618S = companion = southern source. UGC 10182: UGC 10182A = central source, UGC 10182B = southeastern source, UGC 10182C = northeastern source. See Smith et al. 1996 for additional details.

[e] Normal comparison galaxy.

2. STARBURST PROPERTIES

In order to characterize the nature of star formation in starburst systems, we wish to determine the intensity of the current star formation, the age of the starburst, and the environments in which star formation occurs. The following sections discuss the properties selected for this purpose and their implications regarding the intensity, age, and environments of the starbursts. Properties are derived from radio or infrared observations when possible in order to minimize the effects of extinction.

Section 2.1 discusses the global ionizing flux derived from the total 4.85 GHz flux emitted by each galaxy. The ionizing flux provides a measure of the current young massive stellar population, i.e., the intensity of recent star formation. In § 2.2, a comparison of the stellar, Lyα, and far-infrared luminosities of the starbursts assesses the fraction of the total stellar luminosity emitted shortward of the Lyman edge. These data provide additional insights into the intensities of the starbursts by constraining the shapes of the starburst IMFs. Section 2.3 employs near-infrared colors as a probe of the star-forming environment; near-infrared colors measure the relative roles of emission from red and blue stars, thermal gas, and hot dust, as well as the effects of extinction. Section 2.4 places limits upon the ages of the starbursts from the strength of the near-infrared stellar CO absorption features. Finally, § 2.5 analyzes the [N II]/Hα line ratios of the galaxies. A comparison of the line ratios sheds light upon the relative excitation conditions within the star-forming environments.

2.1. *The Ionizing Flux*

The intrinsic number of ionizing photons, $N_{\rm UV}$, places important constraints upon the total number and the mass distribution of hot young massive stars within a galaxy. This quantity is often derived from extinction-corrected recombination line fluxes. This technique cannot be applied with sufficient accuracy to the galaxies in our sample owing to uncertainties in the geometry of the obscuring dust and a lack of multiple recombination line measurements. We therefore use thermal radio fluxes to calculate the number of ionizing photons; extinction at radio wavelengths is presumably negligible.

Standard recombination theory states that the number of ionizing photons is related to the thermal radio flux as

$$N_{\rm UV} = 7.1 \times 10^{49} \left(\frac{D}{1\ {\rm Mpc}}\right)^2 \left(\frac{\nu}{\rm GHz}\right)^{0.1} \left(\frac{T_e}{10^4\ {\rm K}}\right)^{-0.76} S_T(\nu)\ , \quad (1)$$

where $S_T(\nu)$ is the thermal radio flux in mJy, and T_e is the electron temperature. We assume a value of $T_e = 10{,}000$ K. The thermal radio flux for each galaxy is calculated from the 4.85 GHz fluxes provided by CFB91 assuming the empirical relationship between the nonthermal flux ($S_{\rm NT}$) and thermal flux (S_T) given by Condon & Yin (1990):

$$\frac{S_{\rm NT}(\nu)}{S_T(\nu)} \sim 10 \left(\frac{\nu}{1\ {\rm GHz}}\right)^{0.1-\alpha}\ . \quad (2)$$

A value of $\alpha \sim 0.8$ is adopted as a typical nonthermal spectral index. Since equation (2) is derived from *observed* radio and Hα fluxes and represents an average over many cases, thermal radio fluxes derived from equation (2) for *individual* galaxies should be regarded with some caution. A factor of 2 uncertainty is allowed in equation (2) to account for the scatter in the observed radio-Hα correlation (Condon 1992). We consider it unlikely that the galaxies in our sample would possess $S_{\rm NT}/S_T$ ratios outside of this range since their radio properties indicate that their radio emission is dominated by star formation processes. Table 2 lists the estimated thermal radio flux for each galaxy in the sample and the derived number of ionizing photons. We note that the thermal radio flux represents $\sim$25% of the total 4.85 GHz flux. For comparison, the number of ionizing photons is also calculated in the same manner for M82. In the case of M82, the resulting values of $N_{\rm UV}$ are consistent with the value derived by McLeod et al. (1993).

We find that the galaxies in this sample possess an average ionizing luminosity of $N_{\rm UV} = (1.13 \pm 1.18) \times 10^{55}$ s^{-1} and produce 2.6–40 times as many ionizing photons as M82. This result may imply that M82 is a less violent starburst or that M82 is simply a physically smaller system. To assess the nature of the difference between these starbursts and M82 further, we have compared the number of ionizing photons to the far-infrared luminosity ($L_{\rm IR}$). The ratio $N_{\rm UV}/L_{\rm IR}$ should reflect a fundamental property of the burst and not simply trace the size of the system. We note that the far-infrared luminosity approximates the bolometric luminosity in heavily obscured infrared luminous systems such as those studied here. Figure 1 indicates that the $N_{\rm UV}/L_{\rm IR}$ ratio observed in the starbursts scatters about that observed in M82. Although statistically small, the scatter may reflect differences in the stellar populations and/or dust contents of the starbursts. Since $N_{\rm UV}$ is derived directly from the total radio flux, Figure 1 also confirms that both the luminous starbursts and M82 follow the well-known radio–far-infrared correlation characteristic of "normal" star forming galaxies (Helou et al. 1985; Condon et al. 1991a).

2.2. *The Lyα and the Stellar OB Luminosities*

A comparison between the Lyα luminosity ($L_{\rm Ly\alpha}$), the total OB stellar luminosity ($L_{\rm OB}$) and the far-infrared luminosity ($L_{\rm IR}$) provides additional insight into the starburst stellar populations and dust content, as discussed below.

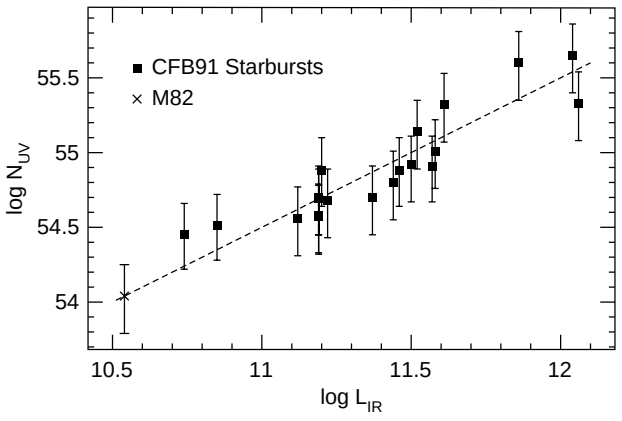

FIG. 1.—Number of ionizing photons. The number of ionizing photons emitted per second ($N_{\rm UV}$), as derived from the 4.85 GHz flux, is plotted as a function of the observed far-infrared luminosity ($L_{\rm IR}$) for each of the 20 radio-luminous starbursts and M82. A dashed line shows the value of $N_{\rm UV}/L_{\rm IR}$ for M82 extrapolated to higher luminosities. The radio-luminous starbursts produce 3–40 times as many ionizing photons as M82. The scatter in the $N_{\rm UV}/L_{\rm IR}$ ratio presumably reflects differences in the starburst stellar populations or dust contents. Both M82 and the radio-luminous starbursts obey the well-known radio and far-infrared correlation.

TABLE 2

THE IONIZING FLUX

GALAXY	S_T(mJy)[a]		log (N_{UV})[b]	
	Nominal[c]	Range[d]	Nominal[c]	Range[d]
UGC 1315	5.89	3.34–9.54	54.92	54.67–55.12
UGC 1655	11.08	6.28–17.93	54.68	54.43–54.89
UGC 2238	8.02	4.54–12.97	54.70	54.45–54.91
UGC 2608	10.37	5.88–16.79	54.88	54.64–55.09
UGC 3334	14.15	8.02–22.90	54.51	54.27–54.72
UGC 3351	10.85	6.15–17.55	54.57	54.32–54.78
UGC 3608	5.89	3.34–9.54	54.56	54.31–54.77
UGC 4509	13.91	7.88–22.51	54.80	54.55–55.01
UGC 4756	6.37	3.61–10.30	55.32	55.07–55.53
UGC 5101	18.63	10.56–30.15	55.60	55.35–55.81
UGC 6471/2.....	70.73	40.09–114.48	55.01	54.76–55.22
UGC 8335	6.37	3.61–10.30	54.91	54.67–55.12
UGC 8387	10.85	6.15–17.55	54.88	54.64–55.09
UGC 8696	24.28	13.77–39.30	55.65	55.41–55.86
UGC 9618	8.96	5.08–14.50	55.14	54.89–55.35
UGC 9913	48.10	27.26–77.84	55.33	55.08–55.54
UGC 10182	9.43	5.35–15.26	54.45	54.21–54.66
UGC 10647	10.61	6.01–17.17	54.69	54.45–54.90
UGC 12332	14.38	8.15–23.28	54.70	54.45–54.91
UGC 12815	14.15	8.02–22.90	54.58	54.33–54.79
M82	1016	576–1645	54.04	53.79–54.25

[a] Thermal flux at 4.85 GHz as calculated from the total 4.85 GHz flux measured by CFB91.

[b] Logarithm of the number of ionizing photons as derived from the thermal radio flux.

[c] Calculated using eq. (2), as given.

[d] Calculated allowing a factor of 2 uncertainty in eq. (2).

The quantity $L_{\mathrm{Ly}\alpha}$ is derived from the thermal radio flux as in Paper I assuming $T_e \sim 10{,}000$ K:

$$L_{\mathrm{Ly}\alpha} = 2.36 \times 10^4 T_e^{-0.45} \frac{S_T(5\ \mathrm{GHz})}{1\ \mathrm{Jy}} \left(\frac{D}{1\ \mathrm{kpc}}\right)^2 L_\odot\ , \quad (3)$$

where S_T(5 GHz) is the thermal 5 GHz flux and D is the distance to the galaxy (Myers et al. 1986).

The OB stellar luminosity is calculated from the number of ionizing photons derived in § 2.1 and simple stellar population models. The bolometric luminosity of the OB stars, L_{OB}, is expressed as

$$L_{\mathrm{OB}} = N_0 \int_{m_l}^{m_u} l(m) m^{-\alpha} t(m) dm\ , \quad (4)$$

where N_0 is a normalization constant representing the number of stars created per year, m_l is the lower mass cutoff of the IMF, m_u is the upper mass cutoff of the IMF, α is the slope of the IMF, $l(m)$ is the bolometric luminosity of a star of mass m, $t(m)$ is the main-sequence lifetime of a star of mass m, and m is in solar masses. We adopt a Miller & Scalo IMF ($\alpha = 3.3$ for $M \geq 10\ M_\odot$; $\alpha = 2.5$ for $1\ M_\odot \leq M \leq 10\ M_\odot$; $\alpha = 1.4$ for $M \leq 1\ M_\odot$) with $m_u = 100\ M_\odot$ and $m_l = 2.6\ M_\odot$. For comparison, a Salpeter IMF is characterized by a slope of $\alpha = 2.35$. Stars with masses below $2.6\ M_\odot$, i.e., stars of spectral type later than A0, are not included since we wish only to calculate the luminosity associated with the OB stars. The quantity $t(m)$, where $t(m)$ is in years, has been parameterized by Larson (1974) as $\log t(m) = 10.02 - 3.57 \log m + 0.9(\log m)^2$. The calibration of $l(m)$ is given by the evolutionary tracks of Maeder & Meynet (1988).

The normalization constant N_0 is derived by comparing the observed values of N_{UV} (see Table 2) with the values predicted by simple stellar population models. Following the discussion of Gehrz, Sramek, & Weedman (1983), the number of ionizing photons, N_{UV}, may be expressed as

$$N_{\mathrm{UV}} = N_0 \int_{m_l}^{m_u} UV(m) m^{-\alpha} t(m) dm\ , \quad (5)$$

where $UV(m)$ is the number of ionizing photons produced by a star of mass m. In this calculation, a lower mass limit of $m_l < 5\ M_\odot$ is assumed. Stars with masses below $5\ M_\odot$ need not be included since they do not produce ionizing photons. The ionizing fluxes quoted by Panagia (1973), the evolutionary tracks of Maeder & Meynet (1988), and the calibration data given by Schmidt-Kaler (1982) determine $UV(m)$. The adopted quantities are summarized in Table 3 for OBA main-sequence stars.

The calculated values of $L_{\mathrm{Ly}\alpha}$, L_{OB}, $L_{\mathrm{IR}}/L_{\mathrm{Ly}\alpha}$, and $L_{\mathrm{OB}}/L_{\mathrm{IR}}$ are presented in Table 4. The results of our calculations are not altered by the use of alternative evolutionary tracks (see, e.g., Schaller et al. 1992). As in § 2.1, a factor of 2 uncertainty is allowed in the derivation of the thermal radio flux. We note that $L_{\mathrm{Ly}\alpha}$ and L_{OB}, and consequently $L_{\mathrm{IR}}/L_{\mathrm{Ly}\alpha}$ and $L_{\mathrm{OB}}/L_{\mathrm{IR}}$, are not independent quantities since they are both derived from the thermal radio flux.

2.2.1. *The Infrared Excess*

The ratio $L_{\mathrm{IR}}/L_{\mathrm{Ly}\alpha}$ is also known as the infrared excess (IRE). Changes in this quantity are due to differences in P_c, the percentage of the total luminosity emitted shortward of the Lyman edge, ϵ, the fraction of Lyman continuum photons absorbed by the gas, and x, the fraction of the absorbed photons that are converted to Lyα photons (see below). The IRE is therefore sensitive to differences in the

TABLE 3

MAIN-SEQUENCE STELLAR PARAMETERS

Spectral Type	Mass ($M_\odot$)	log $T_{\rm eff}$	log $L/L_\odot$	log $N_{\rm UV}$	M_V	M_K
O3	102	4.72	6.15	49.96	−6.00	−5.11
O4	84	4.68	6.00	49.84	−5.90	−5.01
O5	73	4.65	5.90	49.76	−5.70	−4.81
O6	52	4.61	5.62	49.52	−5.50	−4.61
O7	42	4.58	5.41	49.26	−5.20	−4.31
O8	34	4.55	5.23	49.08	−4.90	−4.01
O9	27	4.52	4.99	48.84	−4.50	−3.65
B0	21	4.48	4.72	48.43	−4.00	−3.19
B1	14	4.40	4.20	47.24	−3.20	−2.48
B2	9.8	4.34	3.76	45.74	−2.40	−1.77
B3	7.2	4.27	3.28	44.61	−1.60	−1.06
B5	5.5	4.19	2.92	0.00	−1.20	−0.80
B6	4.9	4.15	2.70	0.00	−0.90	−0.56
B7	4.3	4.11	2.51	0.00	−0.60	−0.33
B8	3.7	4.08	2.26	0.00	−0.20	0.02
B9	3.1	4.02	1.98	0.00	0.20	0.31
A0	2.6	3.98	1.73	0.00	0.60	0.57
A1	2.3	3.97	1.54	0.00	1.00	0.91
A2	2.2	3.95	1.41	0.00	1.30	1.14
A3	2.1	3.94	1.32	0.00	1.50	1.27
A5	2.0	3.91	1.15	0.00	1.90	1.52
A7	1.8	3.89	1.02	0.00	2.20	1.72
A8	1.8	3.88	0.93	0.00	2.40	1.81

stellar mass distribution and the dust and gas content of a star-forming region. This relationship can be understood as follows.

In a dusty star-forming region, three effects can contribute to the observed far-infrared luminosity: (1) the absorption of Lyα photons, (2) the absorption of Lyman continuum photons that have not been converted to Lyα photons, and (3) the absorption of nonionizing photons. We therefore expect

$$L_{\rm IR} = L_{{\rm Ly}\alpha} + (1-\epsilon)P_c L_T + (1-x)\epsilon P_c L_T + (1-P_c)L_T(1-e^{-\tau(\lambda>\lambda_0)}) , \quad (6)$$

where L_T is the total luminosity of the stars, $\tau(\lambda > \lambda_0)$ is the optical depth at wavelengths longer than the Lyman edge, and the obscuring dust is in the form of an overlying screen

TABLE 4

THE OB AND Lyα LUMINOSITIES

	log $L_{\rm OB}$ [a]		log $L_{{\rm Ly}\alpha}$ [b]		$L_{\rm OB}/L_{\rm IR}$		$L_{\rm IR}/L_{{\rm Ly}\alpha}$ [c]	
GALAXY	Nominal[d]	Range[e]	Nominal[d]	Range[e]	Nominal	Range	Nominal	Range
UGC 1315	11.95	11.70–12.15	10.57	10.32–10.78	2.83	1.59–4.49	8.55	5.28–15.08
UGC 1655	11.71	11.46–11.92	10.33	10.08–10.54	3.10	1.75–5.03	7.73	4.78–13.64
UGC 2238	11.73	11.48–11.94	10.35	10.10–10.56	3.48	1.96–5.65	6.93	4.28–12.22
UGC 2608	11.91	11.67–12.12	10.53	10.29–10.74	5.15	2.96–8.35	4.62	2.86–8.15
UGC 3334	11.54	11.30–11.75	10.16	9.92–10.37	4.92	2.83–7.98	4.84	2.99–8.54
UGC 3351	11.60	11.35–11.81	10.22	9.97–10.43	2.58	1.45–4.19	9.38	5.80–16.55
UGC 3608	11.59	11.34–11.80	10.21	9.96–10.42	2.96	1.67–4.81	8.09	5.00–14.27
UGC 4509	11.83	11.58–12.04	10.45	10.20–10.66	2.47	1.39–4.00	9.76	6.03–17.21
UGC 4756	12.35	12.10–12.56	10.97	10.72–11.18	5.52	3.10–8.95	4.39	2.72–7.75
UGC 5101	12.63	12.38–12.84	11.25	11.00–11.46	5.91	3.33–9.59	4.02	2.49–7.10
UGC 6471/2.....	12.04	11.79–12.25	10.66	10.41–10.87	2.90	1.63–4.70	8.39	5.18–14.80
UGC 8335	11.94	11.70–12.15	10.56	10.32–10.77	2.35	1.35–3.82	10.03	6.20–17.70
UGC 8387	11.91	11.67–12.12	10.53	10.29–10.74	2.83	1.63–4.59	8.51	5.26–15.01
UGC 8696	12.68	12.44–12.89	11.31	11.06–11.51	4.38	2.52–7.11	5.49	3.39–9.69
UGC 9618	12.17	11.92–12.38	10.79	10.54–11.00	4.49	2.52–7.28	5.41	3.34–9.54
UGC 9913	12.36	12.11–12.57	10.98	10.73–11.19	2.00	1.13–3.25	12.09	7.47–21.33
UGC 10182	11.48	11.24–11.69	10.10	9.86–10.31	5.52	3.18–8.95	4.35	2.69–7.68
UGC 10647	11.72	11.48–11.93	10.34	10.10–10.55	3.40	1.96–5.52	6.93	4.28–12.22
UGC 12332	11.73	11.48–11.94	10.35	10.11–10.56	2.30	1.29–3.73	10.52	6.50–18.56
UGC 12815	11.61	11.36–11.82	10.23	9.98–10.44	2.64	1.49–4.28	9.19	5.68–16.21
M82	11.07	10.82–11.28	9.69	9.45–9.90	3.40	1.91–5.52	7.01	4.33–12.37

[a] Logarithm of the OB stellar luminosity ($L_\odot$), assuming a Miller and Scalo IMF with $m_u = 100\,M_\odot$ and $m_l < 5\,M_\odot$.
[b] Logarithm of the Lyα luminosity ($L_\odot$).
[c] The infrared excess (§ 2.2.1).
[d] Nominal value, calculated using eq. (2).
[e] Range of values, calculated by incorporating the factor of 2 uncertainty in eq. (2).

(Petrosian, Silk, & Field 1972; Panagia 1974; Ho & Haschick 1981). The overlying dust screen is assumed to be optically thick at wavelengths shorter than the Lyman edge. Equation (7) can be generalized to other dust geometries through the use of a generic variable A, the fraction of the luminosity emitted at $\lambda > \lambda_0$ that is absorbed by dust:

$$L_{\rm IR} = L_{\rm Ly\alpha} + (1 - \epsilon)P_c L_T + (1 - x)\epsilon P_c L_T + (1 - P_c)L_T A \, . \quad (7)$$

Variations in the infrared excess are therefore associated with three factors: (1) differences in the percentage of the total stellar flux emitted shortward of the Lyman edge, and consequently the stellar mass distribution; (2) the fraction of Lyman continuum photons absorbed by the gas and converted to Lyα photons; and (3) the optical depth of the dust. Equation (7) can be applied to starburst galaxies, under the assumption that a starburst can be treated as an ensemble of H II regions. For this sample of starbursts, nearly all of the light produced by the starburst will be absorbed by dust and reemitted in the far-infrared since the bursts are heavily obscured [$\tau(\lambda > \lambda_0) \gg 1$, $A \rightarrow 1$]. This implies that $L_T \sim L_{\rm IR}$, assuming that light from the underlying stellar population does not produce a significant portion of the far-infrared luminosity. Taking $L_{\rm Ly\alpha} = x\epsilon P_c L_T$, equation (7) simplifies to

$$L_{\rm IR}/L_{\rm Ly\alpha} = {\rm IRE} = 1/\epsilon x P_c = \Theta/x P_c \quad (8)$$

in the notation of Panagia (1974) and Myers et al. (1986). The IRE is thus sensitive to the relative numbers of high-mass (ionizing) and low-mass (nonionizing) stars (P_c), and to the fraction of Lyman continuum photons absorbed by the gas and converted to Lyα photons (Θ/x). The quantity Θ/x is a function of the spectral type of the exciting star, the optical depths of the H II region and the circumnebular region, and the electron density n_e (Panagia 1974; Myers et al. 1986). At a fixed optical depth, earlier spectral types are associated with lower infrared excesses.

Figure 2 shows that the infrared excesses of all of the starburst galaxies, including M82, fall within the lower range of values observed for Galactic H II regions. The 20 radio-luminous starbursts are characterized by an average nominal IRE of 7.5 ± 2.4. Allowing for the factor of two uncertainty in equation (2), the minimum average IRE is 4.6 ± 1.5, and the maximum average IRE is 13.2 ± 4.2. All of the starburst IREs (minimum, nominal, and maximum values) are lower than the Galactic H II region mean (IRE = 40) (Scoville & Good 1989). All but one of the IREs are also lower than the median (IRE = 20) value observed for Galactic H II regions. If older stars contribute a significant portion (as much as $\sim$30%) of the far-infrared flux associated with starburst galaxies, as suggested by Calzetti et al. (1995), then the values of $L_{\rm IR}/L_{\rm Ly\alpha}$ associated with the starburst itself would be even lower than indicated in Table 4 and Figure 2. Thus, all of the starburst IREs would fall below the median value observed for Galactic H II regions. We thus conclude that the starburst systems possess IREs that are *lower than those of typical Galactic* H II *regions*. The starburst IREs are also confined to a *narrower range of values* than those of Galactic H II regions.

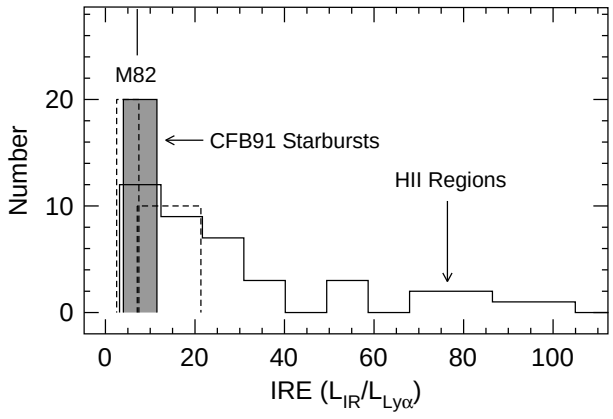

FIG. 2.—Infrared excess. The distribution of the infrared excess (IRE = $L_{\rm IR}/L_{\rm Ly\alpha}$) is shown above for Galactic H II regions, the radio-luminous starbursts, and M82. The shaded region represents the nominal values of the IRE calculated in Table 4. The dashed regions represent the distributions that are obtained when one allows a factor of 2 uncertainty in eq. (2). The starbursts possess IREs that are lower than and confined to a narrower range than those of most H II regions.

In the case of Galactic H II regions, variations in the IRE are primarily associated with changes in the quantity P_c, with larger values of the IRE being associated with the absorption of nonionizing photons emitted by low-mass stars (Ho & Haschick 1981; Myers et al. 1986; Scoville & Good 1989). If variations in P_c are also responsible for the starbursts' comparatively low IREs, then the absorption of nonionizing photons must be less important in the starburst galaxies than in Galactic star-forming regions. This suggests that the stellar light emitted by the starbursts contains a smaller percentage of nonionizing photons or that the optical depths of the starbursts are lower at nonionizing wavelengths. The latter hypothesis can be excluded since the starbursts typically possess high visual optical depths. Therefore, a possible explanation for the observed IREs is that the starburst galaxies possess higher values of P_c. A higher value of P_c will also shift the mean spectral type to an earlier value, which will also decrease the IRE. Differences in either the starburst IMF or the age of the stellar population could produce the higher values of P_c. In the case that the IMFs in the starbursts differ from those in most Galactic H II regions, the observed IREs imply that the starburst IMFs favor the creation of high-mass stars: the upper or lower mass cutoffs may be higher, or the slope may be more shallow. This hypothesis is consistent with studies claiming that the IMF of M82 is biased against the formation of low-mass stars (see, e.g., Rieke et al. 1980, 1993). Alternatively, we may be witnessing an aging effect. Higher values of the IRE will be produced by an aging stellar population since the number of Lyα photons associated with a star-forming region will decrease as the ionizing stars evolve off the main sequence. In comparison to the Milky Way, starburst galaxies may very well possess fewer evolved H II regions and would consequently possess lower IREs. Finally, the starburst star-forming regions may contain more gas than Galactic H II regions and may simply be able to absorb a higher fraction of the Lyman continuum photons. This hypothesis is quite feasible since the starbursts occur in interacting systems and are therefore likely to exist in gas-rich environments.

We suggest that a combination of these effects is responsible for the observed distribution of starburst IREs. The comparatively low IREs can be explained by high values of P_c (and consequently high values of x) and by high values of ϵ. The narrowness of the distribution is more likely to be associated with the quantity P_c since the tail in the

distribution of Galactic H II region IREs is produced by emission from low-mass stars. We therefore conclude that *the absorption of nonionizing photons from low-mass stars appears to play a minor role in powering the infrared emission* from these 20 starbursts. This effect may arise from an IMF that favors the formation of high-mass stars or may indicate that the starbursts contain fewer old H II regions than the Milky Way. The starburst IREs are probably also influenced by the presence of large amounts of gas that absorb a larger fraction of the Lyman continuum photons.

2.2.2. *The L_{OB}/L_{IR} Ratio*

A comparison of L_{OB} and L_{IR} provides additional information regarding the emission properties of these systems. First, a ratio of $L_{OB}/L_{IR} = 1$ indicates that the observed far-infrared flux can be entirely produced by the young O and B stars. A ratio of $L_{OB}/L_{IR} > 1$ implies that some portion of L_{OB} escapes from the galaxy, or that L_{OB} has been overestimated. In the latter case, changing the slope or the mass cutoffs of the IMF to produce an increase in the relative number of high mass stars will lower the value of L_{OB} predicted from a given ionizing flux. Finally, a ratio of $L_{OB}/L_{IR} < 1$ will occur if L_{OB} is underestimated. This situation can arise if Lyman continuum photons are absorbed by dust within the H II regions. In this case, the observed recombination line flux or thermal radio flux will underestimate the Lyman continuum flux originally emitted by the massive stars. Contributions to L_{IR} from low-mass stars or an AGN can also lead to lower values of L_{OB}/L_{IR}. The values of L_{OB}/L_{IR} calculated here should not be affected by an AGN since the selection criteria employed by CFB91 indicate that both the radio luminosity, from which L_{OB} is derived, and the far-infrared luminosity are clearly dominated by star formation processes.

Since the starbursts in this sample are heavily obscured, L_{OB}/L_{IR} should be less than or equal to unity. Table 4 demonstrates that L_{OB}/L_{IR} *exceeds* unity for all of the starbursts; the average value of L_{OB}/L_{IR} is 3.58 ± 1.25. This implies that a significant portion of L_{OB} escapes from these systems or that L_{OB} has been overestimated. The former hypothesis is unlikely given the large optical depths of the star-forming regions. We therefore conclude that *calculations employing a Miller & Scalo IMF overestimate the stellar luminosities associated with a given ionizing luminosity*. To constrain the form of IMF that will produce stellar luminosities consistent with the observed ionizing and far-infrared luminosities, we have varied the value of α for $M \geq 10\ M_\odot$ in equations (4) and (5). Table 5 shows the values of N_0 and α that will produce $L_{OB}/L_{IR} = 1$, as well as the corresponding total star formation rates for $0.1\ M_\odot \leq M \leq 100\ M_\odot$ in units of $M_\odot\ \mathrm{yr}^{-1}$. For the nominal values of N_{UV}, the slopes of the starburst IMFs range from $2.1 \leq \alpha \leq 3.0$, with an average value of 2.7 ± 0.2. The starbursts thus require an IMF that is *more strongly biased toward high-mass star formation* than a Miller & Scalo IMF. For comparison, Hill, Madore, & Freedman (1994) and Massey et al. (1995) find IMF slopes of $\alpha = 3.0 \pm 0.5$ and $\alpha = 2.3 \pm 0.3$, respectively, for Magellanic OB associations. We conclude that the upper mass range of *the starburst IMF bears a strong degree of similarity to that observed in the Magellanic Clouds.*

The calculated star formation rates place rough constraints upon the number of bursts that can be sustained by the host galaxy. Table 5 indicates that the CFB91 starbursts possess an average nominal total star formation rate of $\sim 100\ M_\odot\ \mathrm{yr}^{-1}$. Assuming a constant star formation rate for the entire duration of the burst, a galaxy with $\sim 10^{10}\ M_\odot$ of gas available for star formation could support one

TABLE 5

IMF Parameters for $L_{OB}/L_{IR} = 1$

	N_0[a]		α[b]		SFR[c]	
Galaxy	Nominal[d]	Range[e]	Nominal[d]	Range[e]	Nominal[d]	Range[e]
UGC 1315	48	25–76	2.8	2.5–3.1	132	78–200
UGC 1655	27	10–44	2.8	2.4–3.1	76	33–120
UGC 2238	20	5.1–33	2.7	2.2–3.0	57	19–88
UGC 2608	10	0.07–25	2.4	1.0–2.8	33	6.5–69
UGC 3334	4.3	0.03–10	2.4	1.0–2.8	14	2.8–30
UGC 3351	30	17–48	2.9	2.6–3.2	83	49–130
UGC 3608	21	7.9–33	2.8	2.4–3.1	58	25–89
UGC 4509	51	28–81	2.9	2.6–3.2	140	83–220
UGC 4756	19	0.19–67	2.3	1.0–2.8	66	18–190
UGC 5101	17	0.37–90	2.1	1.0–2.7	73	34–250
UGC 6471/2.....	58	8.6–94	2.8	2.5–3.1	160	26–250
UGC 8335	66	8.8–110	2.9	2.7–3.2	180	25–290
UGC 8387	43	8.5–71	2.8	2.5–3.1	120	26–190
UGC 8696	86	8.4–210	2.5	1.4–2.9	260	190–570
UGC 9618	27	0.19–63	2.5	1.1–2.9	81	12–170
UGC 9913	250	200–380	3.0	2.8–3.3	670	550–1020
UGC 10182	2.6	0.03–9.3	2.3	1.0–2.8	9.0	2.8–26
UGC 10647	20	7.3–33	2.7	2.3–3.0	56	25–88
UGC 12332	41	32–65	2.9	2.7–3.2	110	92–170
UGC 12815	31	17–35	2.9	2.6–3.1	85	50–94
M82	4.4	1.6–7.1	2.7	2.3–3.0	12	5.7–19

[a] Number of stars formed per year.
[b] IMF slope.
[c] Star formation rate ($M_\odot\ \mathrm{yr}^{-1}$).
[d] Calculated from eq. (2), as given.
[e] Calculated by allowing a factor of 2 uncertainty in eq. (2).

such burst for $\sim 10^8$ yr, or 10 bursts of $\sim 10^7$ yr duration. These numbers should be considered cautiously as they depend on several assumptions in addition to a constant star formation rate. All of the gas must be available for star formation and must be converted to stars with 100% efficiency. The estimated number of bursts also depends on the premise that the gas supply is *not* replenished. Finally, the lower mass cutoff of the IMF and the slope of the lower mass range of the IMF will have a strong effect upon the number of bursts that can be accommodated since the majority of the stellar mass resides in low-mass stars.

2.3. *Near-Infrared Colors: 2 μm Emission Mechanisms*

The near-infrared light from "normal" quiescent galaxies is generally dominated by the underlying stellar population, i.e., old, low-mass red giants. In starburst galaxies, young red supergiants (10–20 Myr old intermediate-mass stars) can also contribute a significant portion of the 2 μm light (see, e.g., Devereux 1989; Rieke et al. 1980). Owing to the high luminosities and the low effective temperatures of young red supergiants and old red giants, their emission should account for nearly all of the *stellar* light emitted at 2 μm. Since these evolved red stars have similar near-infrared colors, the intrinsic near-infrared colors of a starburst should then be well defined. Deviations from these characteristic colors reflect changes in the stellar population, the presence of nonstellar emission, and/or extinction effects.

To assess the importance of these effects at 2 μm, we measured the $H-K$ and $J-H$ colors within 2″.5 apertures centered on the nucleus of each starburst galaxy in Paper II. This aperture represents the smallest aperture for which the colors are not adversely affected by seeing changes or sampling and corresponds to a physical size ranging from 0.5 to 2.4 kpc for the galaxies in this sample. The smallest possible aperture is chosen in order to assess the properties of the innermost regions of the starbursts. Since the near-infrared colors of starbursts are often strongly peaked, the colors quickly become diluted in observations utilizing larger beam sizes (Devereux 1989; Paper II). The colors for a 2″.5 aperture are summarized in Table 6 and are displayed in Figure 3. These colors should be regarded as lower limits since the starburst nuclei are not resolved. The colors of two normal spiral galaxies (UGC 8220 and UGC 2085) and those of the companion galaxies to UGC 8335E, UGC 9618N, and UGC 12815 are also indicated. All colors have been corrected for redshift effects and converted to the CIT photometric system, as explained in Papers I and II. Colors for a comoving aperture will be discussed in § 4.

We find that the average colors for the starbursts are $H-K = 0.64 \pm 0.25$ mag and $J-H = 0.87 \pm 0.18$ mag. For comparison, the average colors of other samples found in the literature are shown in Table 7. These colors have been transformed to the CIT photometric system based upon the data given in Bessel & Brett (1988). Since these

TABLE 6

NUCLEAR COLORS OF STARBURST GALAXIES

Galaxy	Θ[a] (pc)	$H-K$ (mag)	$J-H$ (mag)	σ_{H-K} (mag)	σ_{J-H} (mag)	Emission Mechanism[b]
1315	1570	0.43	0.76	0.08	0.06	R, D? (T+D = 4%; B = 3%)
1655	870	0.50	0.77	0.10	0.06	R, B
2238	1050	0.69	1.11	0.08	0.06	R
2608	1140	0.40	0.75	0.08	0.08	R, D? (T+D = 3%; B = 2%)
3334[c]	1370	0.32	0.83	0.01	0.01	R
3351	780	0.60	1.13	0.08	0.08	R (T+D = 1%; B = 5%)
4509	890	0.75	1.02	0.04	0.04	R, B (T+D = 3%; B = 10%)
4756A	2400	0.51	0.71	0.06	0.04	R, B or R, B, D?
4756B.....	2400	0.55	0.72	0.06	0.04	R, B or R, B, D?
4756C	2400	0.38	0.64	0.06	0.06	R, B or R, B, D?
5101	1940	0.94	0.99	0.08	0.06	R, D
6471	500	0.83	1.07	0.06	0.08	R, B (T+D = 8%; B = 20%)
6472B.....	500	0.97	0.96	0.06	0.08	R, D
6472C	500	1.32	0.88	0.06	0.08	R, D
8335E.....	1500	0.73	0.86	0.04	0.04	R, B (T+D = 10%; B = 34%)
8335W[d].....	1530	0.63	0.84	0.04	0.04	R, B
8387	1110	0.80	0.97	0.06	0.06	R, B (T+D = 6%; B = 16%)
8696	1800	0.74	0.89	0.06	0.04	R, D (T+D = 4%; B = 3%)
9618N	1640	0.72	1.02	0.06	0.06	R, B
9618S[d].....	1590	0.28	0.65	0.06	0.06	R
9913	880	0.84	1.20	0.06	0.06	R, B (T+D = 2%; B = 10%)
10182A	730	0.20	0.56	0.06	0.06	R, B or R, B, D?
10182B	730	0.29	0.51	0.06	0.06	R, B or R, B, D?
10182C	730	0.55	0.59	0.06	0.06	R, B or R, B, D?
10647	900	0.57	1.01	0.06	0.04	R
12332	780	0.89	0.88	0.08	0.06	R, D
12813[d].....	670	0.50	0.69	0.10	0.06	R, B or R, B, D?
12815	690	0.52	0.86	0.10	0.06	R, B (T+D = 5%; B = 18%)
M82[e]	70	0.85	1.14	0.05	0.05	R, B (B = 7%)

NOTE.—All colors have been redshift-corrected and transformed to the CIT photometric system.

[a] Colors measured in a 2″.5 aperture.

[b] Emission mechanisms producing $\gtrsim 10\%$ of the observed K-band flux: R = red giants/supergiants, D = hot dust emission, B = blue stars, T = thermal gas. Percentage contributions derived from Brγ fluxes, when available, are given in parentheses.

[c] Colors measured in a 5″.4 aperture by Bushouse & Stanford 1992.

[d] Companion galaxy.

[e] Colors measured in a 4″ × 4″ aperture by Telesco et al. 1991.

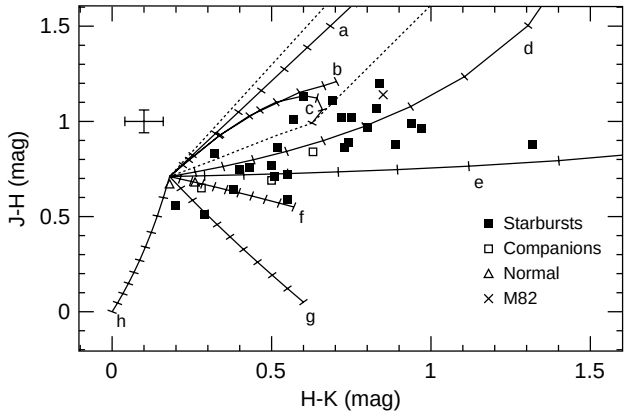

FIG. 3.—Near-infrared colors of starburst nuclei. The colors measured within a 2″.5 nuclear aperture are displayed above with representative uncertainties. The colors of three companion galaxies and two "normal" spiral galaxies are also indicated. For comparison, typical colors of elliptical galaxies would be $H-K = 0.20 \pm 0.05$ and $J-H = 0.68 \pm 0.05$ (see, e.g., Turner et al. 1992). Curves illustrate the effects of (*a*) an external dust screen, (*b*) dust mixed uniformly with stars, (*c*) an obscuring shell of dust, (*d*) dust emission at 1000 K with $\epsilon \propto 1/\lambda$, (*e*) dust emission at 500 K with $\epsilon \propto 1/\lambda$, (*f*) synchrotron emission, (*g*) thermal gas emission from H II regions, and (*h*) blue stars, on the intrinsic colors of evolved red stars. For curves (*d*)–(*h*), tick marks indicate the percentage contribution of each mechanism at *K*, in increments of 10%. For curve (*a*), the interval between tick marks is 1 mag. For curve (*b*), tick marks are shown for $A_V = 1.5$, 6, 10, 20, 30, and 40 mag. For curve (*c*), tick marks are shown for $A_V = 1.5$, 4, 8, 10, 15, 20, 30, and 40 mag. The dotted line outlines the region covered by additional reddening models available in the literature (see Figs. 4 and 5). All measurements and models have been converted to the CIT photometric system. The near-infrared colors of the majority of the starbursts are not consistent with an obscured mixture of evolved red stars. Emission from blue stars, and in some cases hot dust, appears to play an important role in defining the colors of these objects.

data were obtained with a wide variety of beam sizes, the data given in Paper II are also used to tabulate the average colors of the CFB91 starbursts for 5″ and 10″ apertures. Table 7 indicates that the CFB91 starburst nuclei are generally *redder than less luminous starbursts* studied previously in the literature. The starbursts examined here are instead similar in color to those of luminous *IRAS* systems and Seyfert 2 systems. We note that the similarity between the colors of the CFB91 starbursts and the luminous *IRAS* systems is not surprising since several of the CFB91 starbursts are included in the survey of Carico et al. (1988).

To interpret the observed colors, "mixing curves," such as those commonly employed in the literature (see, e.g., Joseph et al. 1984; Telesco et al. 1991; Mazzarella et al. 1992; Larkin et al. 1994), are also shown in Figure 3. These curves illustrate the effects of blue stars, thermal gas emission, synchrotron emission, and hot dust upon the colors of a normal population of evolved red stars. A dotted line outlines the region of the color-color diagram that can be reached by existing reddening models. For clarity, only three of these models are plotted in Figure 3. The reddening vectors for a sphere of uniformly mixed dust and stars and a dust-free sphere of stars surrounded by a clumpy shell of dust are taken from Gordon, Calzetti, & Witt (1997; hereafter GCW) and include the effects of scattering. The less realistic case of an overlying screen of nonscattering obscuring material is also shown. The reddening vectors are derived using the Galactic extinction law $A_K = 0.57A_H = 0.34A_J$ (Whittet 1992). Use of a different extinction law (see, e.g., Cohen et al. 1981; Landini et al. 1984; Draine 1989; Mathis 1990) will not alter the results discussed below since the differences between the various extinction laws are smaller than or comparable to our photometric uncertainties. A more comprehensive illustration of reddening trajectories is given in Figures 4 and 5. These figures include reddening curves associated with shells and spheres of homogenous and clumpy dust with different ratios of interclump to clump medium density (Witt & Gordon 1996) and are taken from GCW and K. D. Gordon (1997, private communication). Cases derived for both the Galactic and Small Magellanic Cloud (SMC) extinction laws are given. A two-screen model that neglects scattering effects [$F_{\rm observed} = F_{\rm intrinsic}(f + e^{-\tau})/e^{g\tau}$], such as that discussed by McLeod et al. (1993) and by Satyapal et al. (1997) for M82, completes the set of curves.

It is apparent from Figure 3 that the colors of many of the starburst galaxies and the companion galaxies *cannot be explained solely in terms of a population of evolved red giants and red supergiants obscured by Milky Way or SMC-like dust distributed in the geometries considered to date.* Similar results are found for the starbursts studied by Devereux (1989) and Glass & Moorwood (1985), as well as for many *IRAS* sources (see, e.g., Carico et al. 1988). In contrast, Telesco et al. (1991) argue that the near-infrared colors of M82 are easily explained by a uniform mixture of dust and red stars.

In analyzing this result, we must first consider the possibility that different dust compositions may be responsible for the observed colors. This issue is addressed in part by the recent work of GCW, who study the nature of the obscuring dust in a sample of 30 UV-bright starburst galaxies with metallicities ranging from 0.1 to 2 solar. Their study indicates that the extinction curves of the starburst galaxies are similar to that of the SMC in that they lack a

TABLE 7

AVERAGE NEAR-INFRARED COLORS

Sample	Source Type	Beam (arcsec)	$H-K$ (mag)	$J-H$ (mag)
This paper	Radio-luminous starbursts	2.5	0.64 ± 0.25	0.87 ± 0.18
		5.0	0.57 ± 0.18	0.81 ± 0.16
		10.0	0.49 ± 0.13	0.75 ± 0.14
Balzano 1983	Nuclear Markarian starbursts	10.3	0.29 ± 0.11	0.65 ± 0.06
Joseph et al. 1984	Interacting starbursts	8, 12	0.32 ± 0.10	0.73 ± 0.13
Glass & Moorwood 1985	Southern H II galaxies	6, 9	0.42 ± 0.14	0.77 ± 0.14
Devereux 1989	Noninteracting spiral starbursts	3.6	0.37 ± 0.08	...
Carico et al. 1988	*IRAS* starbursts + AGN	5, 10	0.56 ± 0.24	0.82 ± 0.15
Glass & Moorwood 1985	Seyfert 1	6, 9	0.77 ± 0.24	0.89 ± 0.10
	Seyfert 2	6, 9	0.55 ± 0.33	0.87 ± 0.27

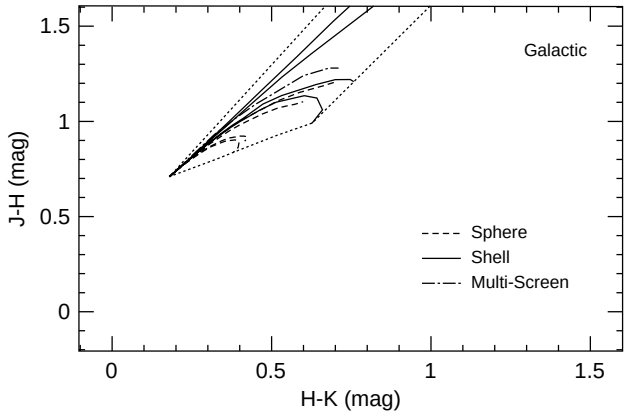

FIG. 4.—Milky Way reddening curves. The reddening trajectories for additional models found in the literature are shown here. A two-screen model that neglects scattering [$F_{\rm observed} = F_{\rm intrinsic}(f + e^{-\tau})/e^{g\tau}$, with $f = 0.3$ and $g = 0.2$], such as discussed by McLeod et al. (1993) and Satyapal et al. (1997), is represented by the dash-dotted line. Models for spheres and shells of dust are taken from GCW and include the effects of scattering. The solid lines portray dust-free spheres of stars surrounded by shells of dust. Cases for a homogeneous shell and for clumpy shells with interclump-to-clump medium-density ratios of $k_2/k_1 = 0.1$, 0.01, and 0.001 (see Witt & Gordon 1996) are shown clockwise from top to bottom. The dashed lines indicate the cases of a sphere of homogeneous dust and spheres of clumpy dust with $k_2/k_1 = 0.1$, 0.01, and 0.001, clockwise from top to bottom. The dotted line outlines the region covered by the reddening models illustrated here and in Fig. 5.

2175 Å bump and rise steeply in the far-ultraviolet. In the near-infrared, however, the differences between the starburst, the Milky Way, and the SMC curves are very small. Given that their starbursts cover a range of metallicities, GCW argue that the observed extinction curves are not linked to metallicity but are due instead to the effects of star formation processes on the distribution of grain sizes and types. These results suggest that our use of the near-infrared portion of the Milky Way and SMC extinction laws is appropriate. However, the fact that the majority of the CFB91 starbursts are more luminous and redder than those studied by GCW may imply that the CFB91 starbursts occur in more extreme environments than the GCW starbursts. Consequently, the possibility that the large grain population that produces the near-infrared portion of the Galactic and the SMC extinction laws is altered in these systems is not necessarily ruled out.

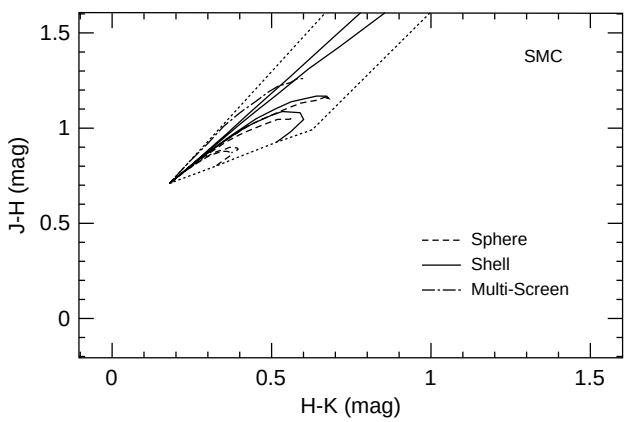

FIG. 5.—Small Magellanic Cloud reddening curves. Same as Fig. 4 for the Small Magellanic Cloud extinction law.

Proceeding with the assumptions that a Galactic or SMC extinction law is appropriate for the CFB91 starbursts and that the true reddening curve lies within the dotted line indicated in Figure 3, we conclude that an emission mechanism other than red stars influences the near-infrared colors of many of the starbursts. The contributions to the 2 μm continuum from other emission mechanisms are constrained as follows. First, synchrotron emission should be negligible at 2 μm since Compton and synchrotron losses will rapidly attenuate the electron spectrum at the required energies. Observations of Galactic H II regions can be used to deduce a relationship between the total 2 μm continuum flux produced by thermal gas and by hot dust and the Brγ flux associated with a star-forming region:

$$\frac{F_{\rm Br\gamma}({\rm W\ cm^{-2}})}{F_{K,\,\rm dust+thermal\ gas}({\rm W\ cm^{-2}\ \mu m^{-1}})} \sim 0.04\ \mu{\rm m} \qquad (9)$$

(Paper I). This relationship can be used in conjunction with the Brγ flux observed from a galaxy to estimate the total amount of thermal gas and hot dust emission. For those galaxies whose Brγ fluxes are quoted in Paper II or the literature, this technique predicts that the average 2 μm continuum flux arising from thermal gas and dust emission, combined, is less than 10% (5% $\pm$ 3%) of the observed K-band flux.

The importance of emission from blue stars at 2 μm can be constrained via the model discussed in § 2.2. The observed K-band flux emitted by the blue OBA stars, F_K(OBA), is expressed as

$$F_K({\rm OBA}) = N_0\, a_K \int_{m_l}^{m_u} f_k(m) m^{-\alpha} t(m) dm\ , \qquad (10)$$

where $f_k(m)$ is the K-band flux of a star of mass m at the distance of the galaxy of interest, and a_K is the fraction of the K-band emission escaping from the galaxy. Values of $f_k(m)$ are derived from the calibrations of Schmidt-Kaler (1982) and Koornneef (1983) (see Table 3). The quantities N_0 and α were determined for each galaxy in § 2.2. The extinction factor, a_K, is derived for 10 of the starburst nuclei and M82 by comparing the observed Brγ fluxes (Paper II; Goldader et al. 1995; Lester et al. 1990) with the intrinsic Brγ fluxes calculated from the thermal radio fluxes $S_T(\nu)$:

$$S_{\rm Br\gamma}({\rm intrinsic}) = 7.8 \times 10^{-15} \left(\frac{\nu}{\rm GHz}\right)^{0.1} \times \left(\frac{T_e}{10^4\ {\rm K}}\right)^{-0.76} \left[\frac{S_{\rm T}(\nu)}{\rm mJy}\right] {\rm ergs\ s^{-1}\ cm^{-2}}\ . \qquad (11)$$

These calculations demonstrate that blue stars produce 2% to $\sim$30% (12% $\pm$ 10%) of the observed K-band fluxes. In the case of M82, we estimate that $\lesssim$ 10% of the nuclear K-band flux is produced by blue stars.

The K-band flux from the starburst galaxies should then be dominated by evolved red stars with *small* contributions from blue stars, thermal gas, and hot dust. If we allow 10%, 5%, and 5% contributions from blue stars, thermal gas, and hot dust, respectively, the intrinsic colors of the starburst will be $H-K \approx 0.23$ mag and $J-H \approx 0.58$ mag. The dotted line that bounds the locus of reddening curves offset to this position is shown in Figure 6. This figure indicates that the nuclear colors of several of the starbursts are consistent with this picture if the starbursts are obscured by

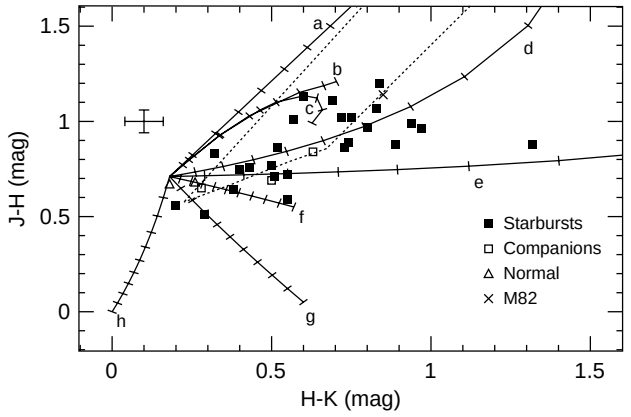

FIG. 6.—Near-infrared colors and the origin of the K-band emission. Same as Fig. 3, except that the origin of the dotted line representing the locus of known reddening curves has been offset to $H-K \approx 0.23$ mag and $J-H \approx 0.58$. These colors are the intrinsic colors of a system where blue stars, H II regions, and hot dust contribute 10%, 5%, and 5%, respectively, of the 2 μm emission. Those starbursts whose $H-K$ and $J-H$ colors lie within the region delineated by the dotted line can be explained by this scenario.

large quantities of dust. While the $J-H$ and $H-K$ colors generally do not provide enough information to identify the exact geometry and composition of the obscuring dust, Figures 4–6 do suggest the following: of the galaxies lying within the region bounded by the dotted line in Figure 6, the nuclei with bluer values of $J-H$ (e.g., UGC 1655 and UGC 12815) are likely to be characterized by clumpy dust distributions. Finally, we caution the reader that there is a known problem with this picture for two of the galaxies lying within the region bounded by the dotted line. The predicted contributions from blue stars for the galaxies UGC 1315 and UGC 2608 are only 3% and 2%, respectively. This problem may be resolved if the attenuation factor a_K in equation (10) is overestimated. Alternatively, a reddening model differing from those in the literature may be required. A moderate contribution from hot dust emission (e.g., $\sim$10%–20%) may also be used to interpret the colors, as discussed below.

In the cases of the remaining galaxies, the $J-H$ colors are too low for their corresponding $H-K$ colors to be explained by this scenario. If the near-infrared colors of some of these objects are to be reproduced with negligible emission from hot dust, then a larger portion ($>10\%$) of the stellar component of the 2 μm continuum flux must arise from blue stars. Again, the starbursts must be heavily obscured ($\tau_V \geq 40$). Table 6 indicates that this explanation is quite feasible for some, but not all, of the galaxies. For example, our calculations predict that blue stars can produce 20% and 34% of the 2 μm emission produced by UGC 6471 and UGC 8335, respectively. Blue stars appear to produce only 3% of the 2 μm emission associated with UGC 8696, however. Finally, a few of the galaxy nuclei possess $H-K$ and $J-H$ colors that are simply too extreme to be explained by even a heavily obscured mixture of young blue and evolved red stars.

An alternative explanation for the observed near-infrared colors involves a nonnegligible contribution from hot dust emission. Glass & Moorwood (1985) and Devereux (1989) have explained the red $H-K$ colors of their starburst samples in terms of a mixture of stellar emission and hot dust emission. Emission from hot dust also appears to play an important role in determining the near-infrared colors of many *IRAS* galaxies (Carico et al. 1988). The observations of Carico et al. (1988) and Zhou, Wynn-Williams, & Sanders (1993) show that many of the starburst galaxies in our sample characterized by red $H-K$ colors also possess red $K-L$ (or $K-L'$) colors. In the absence of an AGN, red $K-L$ colors are most naturally explained in terms of emission from dust heated to temperatures of 500–1000 K by hot young stars (Joseph et al. 1984; Arendt et al. 1994). The dust may be in thermal equilibrium or may be transiently heated. The detection of polycyclic aromatic hydrocarbon (PAH) features in UGC 6472C, M82, and the starburst ring of UGC 12332 provides evidence that hot stars are transiently heating dust to high temperatures (Dudley & Wynn-Williams 1993; Mazzarella et al. 1994; Willner et al. 1977).

If present, an AGN would also be capable of heating dust to high temperatures and thus producing the observed $H-K$ colors. This possibility may explain the similarity between the average colors of the starbursts and those of Seyfert 2 nuclei. The existence of an AGN cannot be ruled out since the criteria employed by CFB91 to distinguish between starbursts and AGNs identify only the *dominant* energy source powering the radio and far-infrared emission and do not rule out the presence of a coexisting low-luminosity AGN. As we will discuss in § 2.5, the evidence supporting the presence of an AGN component in these systems is generally controversial, with the exceptions of UGC 5101 and UGC 12332.

Regardless of the heating mechanism, Figure 3 indicates that the observed colors of many of the CFB91 starburst nuclei are consistent with an obscured mixture of emission from stars and dust at temperatures of 500–1000 K. To explain the colors of the starbursts whose $J-H$ colors are too low, and whose $H-K$ colors are too red to be produced by an obscured mixture of red and blue stars, emission from hot dust would have to produce more than $\sim$5% of the 2 μm continuum light. That is, the amount of dust emission would have to *exceed* that predicted from the Brγ–2 μm flux ratio observed in Galactic H II regions. The amount of dust emission is not necessarily large; a contribution of $\sim$10%–20% from hot dust coupled with those from blue stars and thermal gas is sufficient to explain the colors of many of the starburst nuclei. The exact percentage of 2 μm emission produced by hot dust cannot be determined without knowledge of the temperature of the emitting dust and the geometry and the quantity of obscuring dust. Higher amounts of dust emission are likely to be associated with the starburst nuclei whose $H-K$ colors are very red for their $J-H$ colors.

Assuming that an AGN is not responsible for the excess dust emission in all cases, ionizing photons absorbed within the starburst H II regions may be responsible for some of the excess dust emission. However, large amounts of dust within the H II region would not be consistent with the small observed values of the IRE (§ 2.2.1). The excess dust emission may also arise from areas outside of the H II regions, and the presence of transiently heated small grains is then required. Imaging or spectral observations of the L-band continuum emission and the PAH features at 3.3 μm would place additional constraints upon the nature of the emitting dust in these galaxies. For example, Larkin et al. (1994) have used $JHKL'$ images of M82 to show that $\sim$10% of the K-band emission from the central 1.65 $\times$ 0.32

kpc of M82 is typically produced by hot dust and that emission from hot dust may account for as much as 40% of the K-band emission in certain localized regions of M82. We note that such data are not irrefutable; the reader is referred to McLeod et al. (1993) for an argument against large amounts of hot dust emission in M82 that is based upon spectrophotometry from 1.4 to 4.9 μm. Measurements of multiple recombinations lines in the wavelength regime covered by the $J-H$ and $H-K$ colors, i.e., measurements of the Paβ and Brγ lines, could also aid our understanding of the near-infrared colors by measuring the optical depth toward the ionized gas. The utility of this measurement will be highly dependent upon the geometry of the system; the optical depth toward the ionized gas may differ from the optical depth toward the red stars that dominate the near-infrared continuum emission. Such effects are in fact seen in the ultraviolet and optical spectra of a sample of UV-bright starbursts, where the optical depths derived from recombination lines and from continuum measurements differ by a factor of ~ 2 (Calzetti, Kinney, & Storchi-Bergmann 1994). Calzetti (1997) finds no difference between the optical depths toward the ionizing gas and the stellar continuum in the near-infrared, however. Again, we note that the situation may differ in the redder, more luminous starbursts considered here.

In summary, the following conclusions may be drawn from Figures 3 and 6; these results depend upon the assumptions that a Galactic or SMC extinction law can be applied to the CFB91 starbursts and that the true starburst reddening curve lies within the locus of models depicted in Figure 3. First, the colors of the majority of the starbursts cannot be explained solely by an obscured population of evolved red stars. However, *the colors of many of the starburst nuclei can be understood in terms of heavily obscured emission from evolved red stars, with small contributions from blue stars* ($\approx 10\%$), *thermal gas* ($\approx 5\%$), *and hot dust* ($\approx 5\%$). Several of the starbursts possess $J-H$ colors that are too low, and $H-K$ colors that are too red, to be explained by this scenario. Blue stars may produce as much as $\sim 30\%$ of the 2 μm continuum in some of these objects. Moderate contributions ($\sim 10\%$–20%) from hot dust would also explain many of the observed colors. Finally, those objects with more extreme $H-K$ colors are best explained by larger amounts of hot dust emission. Emission from hot dust may be associated with star formation or in some cases with a low-luminosity AGN.

2.4. CO *Indices and the Red Supergiant Population*

The stellar component of the near-infrared emission should generally be dominated by old red giants, and possibly by young red supergiants. Since young red supergiants represent a specific phase of stellar evolution, their presence or absence has important implications for the age of a starburst. Broadband imaging techniques cannot be used to identify populations of young red supergiants owing to the fact that old red giants and young red supergiants have nearly identical near-infrared colors. Near-infrared spectroscopy can be used to identify young red supergiants, however.

The near-infrared spectra of both old red giants and young red supergiants show CO band head features between 2.3 and 2.4 μm (see, e.g., Kleinmann & Hall 1986). The CO absorption features arise in the photospheres of cool stars and deepen as the temperature and the luminosity of a star decreases and increases, respectively. The strength of the CO band heads, quantified in terms of a photometric or spectrophotometric CO index,[4] thus identifies the stellar population dominating the near-infrared light from a galaxy. For example, elliptical and lenticular galaxies, whose near-infrared light is dominated by red giants, possess an average photometric CO index of $CO_{ph} = 0.155 \pm 0.014$ mag (Frogel et al. 1978). Similarly, late-type spirals are characterized by an average CO index of $CO_{ph} = 0.149 \pm 0.018$ mag (Frogel 1985). A galaxy spectrum dominated by young red supergiants produced from a burst of star formation $\sim 10^7$ yr old would be characterized by a significantly stronger CO index; the prototypical starburst galaxy M82 exhibits a CO index of $CO_{ph} = 0.21$ (McLeod et al. 1993). While enhanced metallicity may also lead to stronger CO absorption features, the presence of young red supergiants remains the most likely explanation for high CO indices in starburst galaxies. For example, stellar population models incorporating metal-rich giants fail to reproduce the CO index observed in M82 (Rieke et al. 1993).

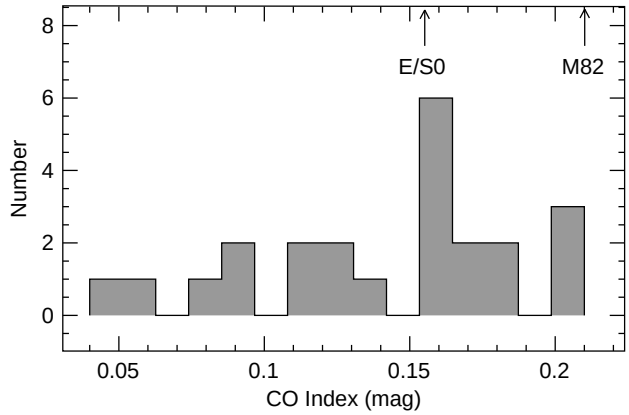

FIG. 7.—CO index. The distribution of CO indices is displayed for the radio-luminous starburst galaxies. Many of the starburst nuclei possess CO indices that are similar to those typically observed in "normal" galaxies ($CO = 0.155 \pm 0.014$ mag). The starbursts with strong CO indices indicate the presence of young red supergiants; these starbursts are at least 10^7 yr old.

To determine if young red supergiants are present in the 20 starburst galaxies and consequently constrain the ages of the bursts, the CO indices derived in Paper II and summarized in Table 8 and Figure 7 are compared to the value observed for "normal" galaxies ($CO_{ph} = 0.155 \pm 0.014$ mag). We note that such comparisons are complicated by the uncertainties inherent in both the measurements and the transformation from spectroscopic CO indices (Paper II) to the photometric CO indices employed by Frogel et al. (1978) and Frogel (1985). Figure 7 indicates that many of the starburst nuclei possess CO indices similar to those observed in E/S0 galaxies but that the starburst nuclei exhibit a wider range of CO indices than E/S0 galaxies. (The average CO index is $CO_{ph} = 0.14 \pm 0.04$ mag.) Three starbursts appear to have stronger than normal CO indices that

[4] The photometric CO index reflects the difference between the magnitudes measured in narrow-band filters centered at 2.2 and 2.36 μm. The CO indices quoted in this paper were measured from spectra and then transformed to a photometric CO index (Paper II).

TABLE 8

CO Indices of Starburst Galaxies and Infrared Luminous Galaxies

Galaxy	$H-K$[a] (mag)	CO_{ph} (mag)
UGC 1315	0.45	0.09 ± 0.03
UGC 1655	0.50	0.11 ± 0.01
UGC 2238	...	...
UGC 2608	0.41	0.16 ± 0.02
UGC 3334	0.32	0.16 ± 0.01
UGC 3351	0.59	0.21 ± 0.02
UGC 3608N	...	0.09 ± 0.02
UGC 3608S	...	0.16 ± 0.02
UGC 4509	0.63	0.17 ± 0.02
UGC 4756B	0.47	0.14 ± 0.02
UGC 5101	0.88	0.08 ± 0.01
UGC 6471	0.67	0.13 ± 0.01
UGC 6472B	0.72	0.13 ± 0.01
UGC 6472C	0.97	0.04 ± 0.01
UGC 8335E	0.59	0.17 ± 0.02
UGC 8335W	0.52	0.20 ± 0.02
UGC 8387	0.68	0.11 ± 0.01
UGC 8696	0.62	0.16 ± 0.01
UGC 9618	0.64	0.16 ± 0.02
UGC 9913	0.67	0.18 ± 0.02
UGC 10182	...	...
UGC 10647	0.55	0.16 ± 0.02
UGC 12332	0.77	0.06 ± 0.02
UGC 12815	0.53	0.18 ± 0.02
UGC 1248	...	0.18 ± 0.02
M82[b]	0.64	0.21 ± 0.01
NGC 520[c]	0.93	0.18 ± 0.05
NGC 1614[c]	0.42	0.20 ± 0.03
IRAS 05189−2524[c]	1.12	0.04 ± 0.03
MGC +00-29-023[c]	0.44	0.15 ± 0.03
NGC 3690B1[c]	0.72	0.08 ± 0.03
NGC 3690B2[c]	0.72	0.21 ± 0.05
NGC 4418[c]	0.26	0.17 ± 0.03
Mrk 231[c]	1.17	0.00 ± 0.03
IRAS 1533−0513[c]	0.53	0.25 ± 0.05
NGC 6090[c]	0.33	0.22 ± 0.03
NGC 6240[c]	0.59	0.21 ± 0.05
MGC +01-42-088[c]	0.41	0.18 ± 0.05
Mrk 331[c]	0.36	0.21 ± 0.03

[a] $H-K$ color measured in a 5″ aperture (Smith et al. 1996; Ridgway et al. 1994).
[b] McLeod et al. 1993.
[c] Ridgway et al. 1994.

are similar to the CO index in M82, and several starbursts are characterized by abnormally low CO indices. UGC 1248, a comparison spiral galaxy, also appears to possess a relatively high CO index. This galaxy is the largest and one of the brightest objects in the cluster A262, and is also characterized by an H I deficiency and an unusually large H I velocity width (Giovanelli, Haynes, & Chincarini 1982). Owing to these unusual properties, UGC 1248 should not be regarded as a "normal" quiescent galaxy. The relatively strong CO absorption features observed in this galaxy may indicate that an episode of star formation has recently taken place.

While the nuclei with strong CO indices presumably contain K and/or M supergiants and consequently possess starbursts that are at least $\sim 10^7$ yr old, the interpretation of the CO indices observed in the remaining galaxies is complicated. The stellar component of those galaxies with a "normal" CO index appears to be dominated by red giants. These systems may contain young ($< 10^7$ yr old) starbursts that have not yet formed supergiants, or old ($> 10^8$ yr old) starbursts in which the supergiants have already died. We note that the presence of nonthermal radio emission associated with supernovae implies that the burst must be at least 4–8 Myr old. In cases in which the CO index is abnormally low, the apparent absence of red giants must also be explained. These galaxies may either be too young to have formed red giants or be characterized by an IMF biased against low-mass star formation $\sim 10^9$ to $\sim 10^{10}$ yr ago. Given that these objects are undergoing a burst of massive star formation, however, a more feasible explanation is that the CO absorption features in the galaxies characterized by normal or below normal CO indices may simply be diluted by light from blue stars or from nonstellar emission.

The possibility of contamination from blue stars or nonstellar emission is in fact quite likely. As discussed in § 2.3, blue stars are capable of producing as much as ∼30% (12% ± 10%) of the 2 μm emission emitted by the starbursts. Emission from hot dust may also produce a nonnegligible fraction of the observed K-band flux in some cases. The effect of dust emission upon the CO index can be quite strong . For example, an equal mixture of emission from a M3–4 type supergiant ($CO_{ph} = 0.33$ mag) and from dust at 1000 K will produce a composite spectrum with a CO index of 0.11 mag. The effect is even stronger if the dust is at a temperature of 500 K; the composite spectrum will have a CO index of 0.05 mag. Emission from blue stars will dilute the CO index in a similar manner.

To assess the influence of diluting mechanisms upon the starburst spectra, the observed photometric CO index is shown with the $H-K$ color measured in a 5″ aperture in Figure 8. For comparison, observations of a sample of infrared-luminous galaxies are also shown (Ridgway, Wynn-Williams, & Becklin 1994). These infrared sources represent another set of luminous systems containing starbursts and/or AGNs. As such, they reflect another set of objects whose CO indices may also be contaminated by emission from blue stars and/or hot dust. Ridgway et al. (1994) conclude that the CO index becomes stronger as the $H-K$ color increases for $0.4 < H-K < 0.8$ and then decreases as the $H-K$ color increases beyond $H-K = 0.8$. The strong CO indices and their associated $H-K$ colors are interpreted in terms of a reddened stellar population containing red supergiants or metal-rich red giants. The

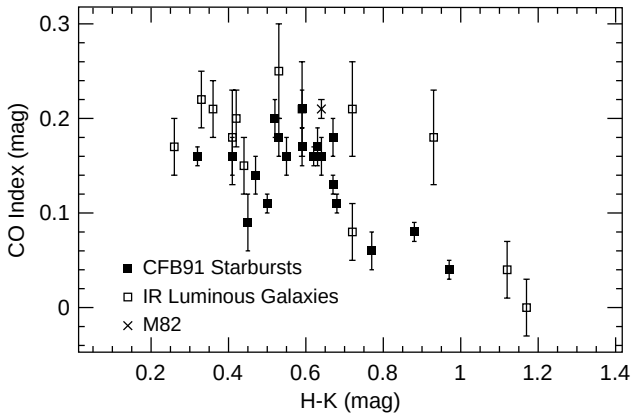

Fig. 8.—CO indices and the $H-K$ color. The CO indices observed for the starbursts are shown above as a function of the $H-K$ color measured in a 5″ aperture. For comparison, the CO indices of a sample of infrared-luminous galaxies are also displayed (Ridgway et al. 1994). The CO indices of galaxies with very red $H-K$ colors are probably diluted by emission from hot dust.

weak CO indices observed at very red values of $H-K$ are thought to be diluted by nonstellar emission. Our data support the trend at red values of $H-K$, i.e., the reddest galaxies in our sample also have the weakest CO indices. Two of these galaxies (UGC 5101 and UGC 12332) appear to contain AGNs; the third galaxy (UGC 6472C) exhibits no evidence of AGN activity. PAH features are present in both UGC 6472C and UGC 12332 (see § 2.3.) We therefore conclude that the CO indices of very red galaxies are diluted by dust heated to high temperatures by intense star formation or by an AGN.

At lower values of $H-K$, we do not see any strong trends in the data. This situation probably reflects the diversity of the star-forming environments. The near-infrared emission from many of the starbursts with lower values of $H-K$ can be explained primarily in terms of an obscured mixture of red and blue stars, as discussed in § 2.3. Since the $H-K$ color resulting from such a stellar population will depend upon both the amount of blue stellar light and the level of obscuration, galaxies with different stellar populations (and different CO indices) can easily have similar $H-K$ colors. Emission from hot dust may also contribute $\sim$10%–20% of the K-band flux associated with some of these galaxies. This level of dust emission will dilute the observed CO indices, although the effect will certainly be less dramatic than in those galaxies with very red $H-K$ colors. The dilution may be difficult to link to the $H-K$ color since the 2 μm light from two starbursts with similar $H-K$ colors may represent similar amounts of hot dust emission at two different temperatures (see Fig. 3). The galaxy whose dust is emitting at the lower temperature will have a lower CO index.

We conclude that the observed CO indices represent *lower limits* to the intrinsic CO indices associated with these systems. The CO indices of those galaxies characterized by very red $H-K$ colors appear to be diluted by nonstellar emission. The CO indices of the starburst nuclei with less extreme $H-K$ colors are likely to be affected by emission from blue stars and possibly hot dust. This effect also explains why many of the CFB91 starbursts possess CO indices that are lower than that of M82. The near-infrared emission from M82 appears to be produced primarily by obscured red stars; the contributions from obscured blue stars and hot dust are quite small. As a result, the CO index observed in M82 should be close to its intrinsic value. The majority of the CFB91 starbursts, however, show evidence for stronger contributions from emission from obscured blue stars and possibly hot dust. The observed CO indices for these galaxies are thus expected to be further from their intrinsic values. We note that the intrinsic values cannot be derived at this time since knowledge of the relative amounts and the geometries of the stars and the emitting and obscuring dust would be required to correct the CO index for the effects of blue stars and hot dust, as well as extinction. These factors are poorly understood owing to the complexity of these systems. The fact that well-constrained optical depths are not available for the majority of the starbursts further complicates the problem. A correction for these effects is therefore postponed until the dust contents of these systems are better constrained. As a result, the observed CO index does not immediately confirm or rule out the presence of red supergiants in many of these galaxies. Finally, we note that the tendency for the CO index to decrease in galaxies with very red $H-K$ colors is the only correlation involving the CO index that is observed in this data set.

2.5. *Optical Emission Lines: Photoionization, Shocks, and AGNs*

Since optical emission-line ratios reflect local excitation conditions, they can be used to identify the dominant energy source within a galaxy (Baldwin, Phillips, & Terlevich 1981; Veilleux & Osterbrock 1987), with the caveat that optical wavelengths may not see a heavily obscured starburst or AGN. Regions dominated by stellar photoionization trace a well-defined locus in a plot of the [O III]/Hβ line ratio versus the [N II]/Hα line ratio. Scatter about this locus is generally attributed to variations in the excitation conditions and in the abundances of the H II regions. In such a diagram, objects dominated by nonstellar high-excitation processes will possess high [O III]/Hβ and high [N II]/Hα line ratios. Our sample is defined to contain only galaxies whose radio and far-infrared fluxes indicate that they are dominated by star formation processes. In this case, optical line ratios are of interest for the purposes of confirming this classification and for investigating the range of ionizing conditions present in starbursts.

We therefore used the long-slit high-resolution spectra that were originally obtained for rotation curve measurements to extract spectra of the galaxy nuclei within 2.4 kpc apertures. This aperture size corresponds to the physical size of the smallest aperture for which we can measure the near-infrared colors of the highest redshift galaxy in the sample (see also § 4.1). The [N II]/Hα line ratios were determined by fitting Gaussians to the Hα and [N II] lines within IRAF,[5] the Image Reduction and Analysis Facility. For the few galaxies characterized by broad line widths, the emission lines were first deblended within IRAF. Flux ratios utilizing widely spaced lines such as Hα/Hβ and [O III]/Hβ ratios were not calculated since our original observations were not obtained for this purpose and were not flux calibrated or corrected for atmospheric extinction. The derived [N II]/Hα line ratios are listed in Table 9. Line ratios for some of the galaxies that we did not observe may be found in Veilleux et al. (1995).

To determine whether the observed [N II]/H α line ratios are consistent with those expected for galaxies dominated by star formation, we assume that the division between galaxies dominated by stellar and nonstellar processes occurs at log ([N II]/Hα) ~ -0.2 (Veilleux & Osterbrock 1987). The line ratios of six galaxies appear to be consistent with star formation processes but indicate a *wide range of star-forming conditions*. Those galaxies with comparatively high [N II]/Hα line ratios may possess lower nitrogen abundances, more emission from shock-heated gas, hotter stars and lower ionization parameters, and/or stellar populations characterized by a larger fraction of stars with Balmer-line absorption features. Alternatively, the spectra of these galaxies may be modified by large amounts of dust embedded within metal-rich H II regions (Shields & Kennicutt 1995). This latter scenario is not consistent with the small observed values of the IRE, however (§ 2.2.1). The remaining galaxies have log ([N II]/Hα) ≥ 0; these galaxies have ionization conditions more consistent with those seen in LINERs or Seyfert galaxies. In summary, in the 16 systems with optical line ratios derived here or published elsewhere,

[5] IRAF is distributed by the National Optical Astronomy Observatories, which are operated by AURA, Inc. under a cooperative agreement with the National Science Foundation.

TABLE 9

OPTICAL PROPERTIES OF STARBURST NUCLEI

	Nucleus		+4.8 kpc		−4.8 kpc	
Galaxy	Width[a]	log ([N II]/Hα)	Width	log ([N II]/Hα)	Width	log ([N II]/Hα)
UGC 4509 (M).....	360	0.03	200	0.39	180	0.13
UGC 4509 (m)	430	−0.01	170	0.01	160	0.36
UGC 4756B	170	−0.62	180	−0.44	160	−0.65
UGC 5101 (M).....	470	0.06	200	−0.28	140	−0.35
UGC 5101 (m)	400	0.25	400	−0.25	240	−0.10
UGC 8335E	200	−0.42	330	−0.37	170	−0.44
UGC 8335W	150	−0.43	280	−0.33	190	−0.41
UGC 8387 (M).....	270	−0.22	240	−0.20	230	−0.07
UGC 8387 (m)	220	−0.17	310	0.03	250	0.09
UGC 8696.....	470	0.02	320	0.29	530	−0.05
UGC 9618N	170	−0.34	280	−0.20	210	−0.19
UGC 9618S	160	−0.43	150	−0.43	150	−0.45
UGC 9913 (M).....	440	0.35	310	0.44	270	0.06
UGC 9913 (m)	380	0.34	320	0.37	290	0.86
UGC 10182	180	−0.67	120	−0.76	130	−0.84
UGC 10647	240	−0.22	150	−0.26	250	−0.13

NOTE.—M = major axis; m = minor axis.
[a] Width = FWHM of Hα emission in km s^{-1}

seven systems show evidence of LINER activity, three objects exhibit Seyfert behavior, and the remaining six galaxies have line ratios consistent with pure star formation activity (see Table 10).

The interpretation of LINER/Seyfert optical line ratios is controversial (see, e.g., Veilleux et al. 1995, and references therein; Filippenko 1989, and references therein; Condon & Broderick 1988, and references therein). Objects exhibiting LINER-type line ratios may be powered by a weak AGN (Ho, Filippenko, & Sargent 1993, and references therein), shocks produced by superwinds associated with outflowing gas and/or collisions between galaxies (Heckman, Armus, & Miley 1990, and references therein), extremely hot high-metallicity Wolf-Rayet stars ("warmers") (Terlevich &

TABLE 10

EVIDENCE FOR AN AGN COMPONENT

Galaxy	Optical[a]	References[b]	8.44 GHz VLA[c]	VLBI[d]	Energy Source
1315	H	1	Extended	...	H II
1655	...	...	...	...	H II
2238	L?	1	...	...	H II
2608	Sy2	2	...	...	H II + possible AGN
3334	...	...	...	...	H II
3351	...	...	...	...	H II
3608	...	...	...	...	H II
4509	L	3, 4	CSB	High T_b	H II + possible AGN
4756	H	4	...	...	H II
5101	L	1, 4	CSB	High T_b; AGN	H II + AGN
6471	H	3	Extended	High T_b	H II + possible AGN
6472B	H	3	Extended	...	H II
6472C	H	3	Extended	...	H II
8335E	H	1, 4	Extended	low T_b	H II
8335W.....	H	1, 4	Extended	...	H II
8387	L/H	1, 4	Extended	low T_b	H II
8696	L	1, 4	CSB	High T_b	H II + possible AGN
9618N	L/H	1, 4	Extended	...	H II
9913	Sy2	1, 4	CSB	High T_b	H II + possible AGN
10182.....	H	4, 5	...	...	H II
10647.....	L/H	1, 4	Extended	intermediate T_b	H II
12332.....	Sy1	1	Extended	High T_b; AGN	H II + AGN
12815.....	H	1	...	...	H II

[a] Classification based upon optical line ratios and the method of Veilleux & Osterbrock 1987. H = H II region; L = LINER; Sy1 = Seyfert 1; Sy2 = Seyfert 2.
[b] SOURCE OF OPTICAL LINE RATIOS.—(1) Veilleux et al. 1995; (2) Mazzarella & Balzano 1986; (3) Armus, Heckman, & Miley 1989; (4) this paper; (5) Ashby, Houck, & Matthews 1995.
[c] Classification of the 8.44 GHz emission mapped by Condon et al. 1991c. "Extended" implies a resolved source and extended emission. "CSB" implies a barely resolved, compact source interpreted as a compact starburst.
[d] Results of VLBI observations by Lonsdale et al. 1993. "High T_b" implies a brightness temperature above 10^7 K. These sources could be powered by either AGNs or luminous supernovae, except in the cases of UGC 5101 and UGC 12332 (Lonsdale et al. 1995). "Low T_b" implies a brightness temperature below 10^5 K. The emission from these objects is driven by star formation processes.

Melnick 1985), and/or cooling flows (see, e.g., Heckman 1981). Some authors have also argued that Seyfert spectra may be associated with compact supernovae remnants formed in a starburst instead of an AGN (see, e.g., Terlevich et al. 1995, and references therein).

We have used the recent work of Veilleux et al. (1995) and high-resolution radio studies to constrain the properties of these objects further. Emission from the LINER objects has been interpreted in terms of shocks induced by an outflow of nuclear gas or interactions between galaxies (Veilleux et al. 1995). In the case of the CFB91 starbursts, this interpretation seems quite feasible since these objects are experiencing tremendous bursts of star formation triggered by violent galaxy-galaxy interactions and mergers. Additional evidence supporting the starburst interpretation of LINER and Seyfert line ratios is found in Condon et al. (1991c). These authors have obtained high-resolution radio maps of the majority of the galaxies in this sample characterized by LINER- or Seyfert-type optical spectra. Their data indicate that the galaxies are powered by extremely compact and dense starburst activity. In contrast, Lonsdale, Smith, & Lonsdale (1993) have detected high brightness temperature structures in six of these galaxies with VLBI. While these authors are unable to clearly distinguish between scenarios involving luminous supernovae and AGNs, Lonsdale, Lonsdale, & Smith (1995) conclude that energy considerations do favor the presence of an AGN in two of the galaxies (UGC 5101 and UGC 12332). Table 10 summarizes the evidence concerning the presence of an AGN for each galaxy in our sample. With the exceptions of UGC 5101 and UGC 12332, we conclude that *the optical emission properties of the galaxies are most likely associated with violent starburst activity triggered by galaxy-galaxy interactions and mergers.* The presence of LINER and Seyfert line ratios testifies to the extreme environments found in some of these galaxies. The fact that some of the galaxies exhibit LINER- or Seyfert-type line ratios complicates efforts to determine their optical depths from standard recombination theory.

3. THE OFF-NUCLEAR REGIONS

We now consider the properties of the disks of the galaxies hosting the starbursts in order to assess the relationship between the nuclear and off-nuclear regions of the starburst. Section 3.1 uses the near-infrared colors of the off-nuclear regions as a tracer of enhanced star formation activity in the host galaxy. Section 3.2 discusses the excitation conditions in the disks of the starbursts systems as derived from the [N II]/Hα line ratio. Finally, § 3.3 analyzes the dynamics of the systems in order to trace the effects of interactions and the circumstances under which enhanced star formation occurs.

3.1. *Near-Infrared Colors of the Disk*

Since the near-infrared colors of "normal" spiral galaxies remain fairly constant across their disks (Paper II; Tendrup et al. 1994), deviations from the characteristic colors of evolved stars also serve as an indicator of recent star formation activity in the disks of galaxies. The peripheral colors of the starbursts can therefore be used as a diagnostic of enhanced star formation, assuming the progenitor galaxies of the observed starburst systems were spirals. The colors of the starburst galaxies derived in Paper II for an annulus with inner and outer diameters of 15″ and 20″, respectively, are therefore presented in Figure 9. At the mean redshift of the sample (94.3 Mpc; $H_0 = 75$ km s^{-1} Mpc^{-1}), the diameters of this annulus correspond to 6.8 and 9.1 kpc. This annular aperture is chosen so that the properties of the near-infrared emission can be studied as far out into the disk as possible, based upon the image quality for the most distant starburst. The near-infrared characteristics of a comoving annular aperture will be discussed in § 4.

The average colors for the peripheral regions are $H-K = 0.34 \pm 0.10$ and $J-H = 0.64 \pm 0.09$ mag. For comparison, typical colors of spiral galaxies are $H-K = 0.24 \pm 0.08$ mag and $J-H = 0.72 \pm 0.08$ mag (Mazzarella et al. 1992). The peripheral regions of the starbursts tend to be characterized by $H-K$ colors that are redder and $J-H$ colors that are bluer than those of "normal" spiral galaxies. Under the assumptions that the dust in these regions is characterized by a Galactic or SMC-like extinction law in the near-infrared and that the true reddening curve lies within the region bounded by the dotted line in Figure 9, it appears that the $H-K$ and $J-H$ colors in the majority of the peripheral regions cannot be produced solely by an obscured population of evolved red stars (see also § 2.3). However, the colors can be explained by an obscured population of evolved red stars and young blue stars. Small amounts of thermal gas emission and hot dust emission may also be present. In contrast, the colors observed in the outer regions of M82 and other M82-type starbursts are more similar to those of spiral galaxies (Larkin et al. 1994; Devereux 1989; Telesco et al. 1991; Aaronson 1977).

Since the off-nuclear near-infrared colors of the CFB91 starbursts differ from those of "normal" spirals and those of less luminous starbursts, we suggest that the *peripheral* regions of the starburst galaxies in our sample exhibit greater levels of star formation activity, i.e., *the starburst activity is not strictly confined to the nuclear regions* of the galaxies. This interpretation of the observed colors depends upon the assumption that the reddening curve obeyed by the disks of the galaxies lies within the dotted region outlined in Figure 9. In this scenario, the fact that the peripheral regions are characterized by a narrower, bluer range of $H-K$ color than the nuclear regions (see Fig. 3) indicates that the star formation activity associated with the periph-

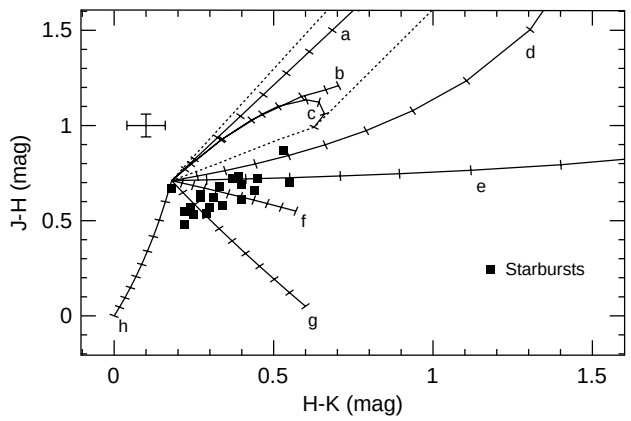

FIG. 9.—Off-nuclear colors. The near-infrared colors observed in an annulus with inner and outer diameters of 15″ and 20″ and representative uncertainties are plotted with the mixing curves discussed in Fig. 3. Like the nuclear colors, these colors cannot be explained solely in terms of evolved stars and reddening. The disks of the starburst galaxies thus appear to be active sites of star formation.

eral regions is *less extreme* and is also *more uniform in nature* from galaxy to galaxy than that occurring in the nuclear regions. The relationship between the nuclear and off-nuclear properties of the CFB91 starbursts will be discussed in more detail in § 4.

Stronger evidence for spatially extended star formation activity is found in the radio. Radio maps obtained by Condon et al. (1990) and by CFB91 at 1.49 GHz and at 4.85 GHz, respectively, indicate that the spatial extents of the radio emission associated with the CFB91 starbursts range from 0.7 to 14 kpc along the major axes of UGC 9913 and UGC 12815, respectively. For comparison, the spatial extent of the 1.49 GHz emission associated with M82 is only 0.6 kpc along the major axis (Condon et al. 1990). We conclude that the peripheral regions of M82 and other starbursts of similar luminosity are characterized by "normal" levels of star formation activity. In contrast to the CFB91 starbursts, the M82-type starbursts are confined to a small nuclear region.

The observed differences between the CFB91 starbursts and the M82-type starbursts may arise in two different manners. The mechanism responsible for triggering the starbursts simply may not be able to trigger spatially extended starburst activity in less-luminous systems such as M82. Alternatively, we may be witnessing the evolution of a spatially extended starburst. This scenario assumes that all starbursts will extend beyond the nuclear region at some point in their evolution. Nuclear starbursts then represent systems whose disk component has already died or has not yet occurred.

3.2. *Optical Emission-Line Properties*

To study the relationship between the excitation conditions in the nuclear and the off-nuclear star forming regions, the [N II]/Hα flux ratios were measured in 2.4 kpc apertures centered ±4.8 kpc from the nucleus. We note that a correlation between the line ratios is not necessarily expected since the star-forming environment appears to be more extreme in the nuclear regions than in the off-nuclear regions. A linear fit to the combined [N II]/Hα line ratio data compiled in Table 9 is shown in Figure 10. The data imply that the line ratio observed on the nucleus is correlated with that observed 4.8 kpc off the nucleus. The probability that this correlation could arise from a random distribution is $\sim 10^{-5}$%. We note that some of the off-nuclear line ratios are consistent with LINER activity. This suggests that the mechanism responsible for LINER-type line ratios in starburst systems is not strictly confined to the galaxy nucleus. The data thus argue in favor of a spatially extended excitation mechanism such as shock excitation resulting from nuclear outflow or galaxy-galaxy interactions (see, e.g., Veilleux et al. 1995, and references therein).

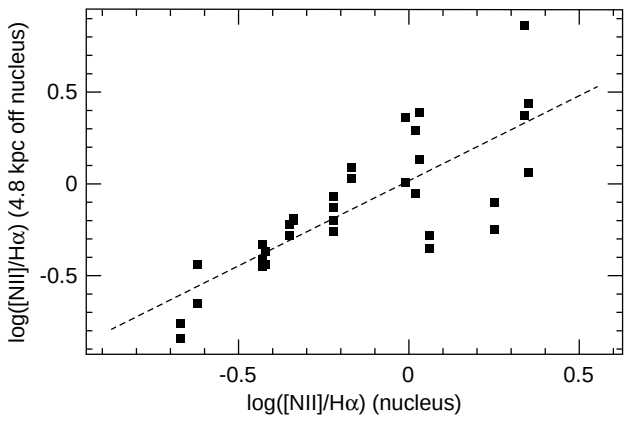

FIG. 10.—Optical line ratios. The value of the [N II]/Hα line ratio is indicated for apertures centered on the starburst nucleus and ±4.8 kpc from the nucleus. The line represents a least-squares linear fit to the data. Owing to the high optical depths of these galaxies, the "nuclear" line ratio most likely represents regions along the line of site to the starburst nucleus. The galaxies hosting the starbursts exhibit a range of excitation conditions; the excitation conditions are fairly constant across any given galaxy.

The interpretation of the correlation between the nuclear and off-nuclear line ratios depends upon the optical depths of the starburst nuclei. For heavily obscured systems, the fluxes within the "nuclear" apertures are probably dominated by regions in the disk of the host galaxy that lie *along the line of site* to the starburst nucleus, depending upon the galaxy inclination angle. The fact that the "nuclear" and off-nuclear [N II]/Hα line ratios are positively correlated indicates that *the excitation conditions do not vary significantly across the disk of the galaxy* in this case. For less heavily obscured systems, the correlation suggests that the excitation conditions are similar in the off-nuclear and the nuclear regions.

Figure 10 also shows an increase in the scatter of the data as the [N II]/Hα line ratio increases. This effect implies that the excitation conditions in the on and off-nuclear regions of the starbursts characterized by LINER- or Seyfert-type spectra are not as closely related as in starbursts possessing "normal" [N II]/Hα line ratios. This effect is also seen in infrared luminous galaxies possessing LINER or Seyfert spectra (Veilleux et al. 1995). The scatter in the line ratios is most likely associated with the variety of physical environments present in these objects, and perhaps optical depth effects. Objects with LINER or Seyfert nuclear spectra will exhibit a variety of off-nuclear line ratios, depending upon whether the nuclear emission is powered by shocks, extremely hot stars, or an AGN. For example, UGC 8387 possesses a LINER-type optical spectrum that is presumably produced by shock excitation (Veilleux et al. 1995). Our data show that both the [N II]/Hα line ratio and the Hα FWHM *increase* along the minor axis of UGC 8387. The rotation curve along the minor axis also displays unusual behavior: the observed velocity of the Hα emission changes by 200 km s^{-1}. In contrast, normal galaxies typically show velocity dispersions of ~ 50 km s^{-1} along the minor axis. The increasing [N II]/Hα line ratio, Hα FWHM, and velocity are all consistent with the presence of a superwind created by supernovae explosions (Heckman et al. 1990). In contrast, UGC 5101 appears to contain both an AGN and a starburst. The nuclear [N II]/Hα line ratio reflects the AGN activity. The off-nuclear [N II]/Hα line ratios become more H II region–like, reflecting the starburst activity. The tightness of the relationship between the nuclear and off-nuclear line ratios in the systems whose line ratios are fairly low is presumably due to the fact that the emission on and off the nucleus is dominated by stellar photoionization. In optically thick systems, the tightness of the correlation may also be due to the fact that the nuclear aperture will sample regions along the line of sight to the nucleus. These areas may very well lie at the same radius as the off-nuclear regions. We conclude that *the off-nuclear regions of the starburst systems exhibit a variety of star-forming conditions* reflecting the excitation mechanism powering the nuclear emission.

3.3. *Dynamical Behavior*

The dynamical behavior of the galaxy hosting a starburst provides important clues regarding the method by which the burst is triggered and fueled. For example, a stellar bar will produce noncircular motions. In interacting systems, the presence or absence of noncircular motions reflects the age of the interaction and the degree of disturbance within the host galaxy.

In Paper II, Hα rotation curves were derived for 10 of the starbursts in order to determine a typical dynamical mass for these systems. Here, we return to these data to analyze the dynamical behavior of the starburst galaxies. Rotation curves can be classified as one of three types: normal, solid-body, or barred. In a "normal" system, the rotation curve flattens in the outer regions. In contrast, a "solid-body"–type rotation curve exhibits rotational velocities that increase linearly with radius. A "barred" system will possess a rotation curve that rises steeply in the inner regions of the galaxy, reaches a maximum, and then declines and flattens. We note that this classification scheme can become complicated at high optical depths. It is thought that the Hα rotation curves of optically thick systems should be characterized by solid-body rotation since the detected Hα emission arises from the outer disk (Goad & Roberts 1981). Since recent models indicate that this effect is markedly reduced at inclination angles as little as 5° from edge-on, the majority of our galaxies should not be affected, however (Bosma et al. 1992).

Several of the rotation curves presented in Paper II do show evidence of noncircular gas motions as noted in Table 11. The presence of noncircular motions is most evident in the western nucleus of UGC 8335; the rotation curve of this object bears a striking resemblance to those of spiral galaxies possessing an inner bar. In other galaxies, one side of the rotation curve flattens, while the other side shows evidence for a turn similar to that seen in UGC 8335W. Two galaxies show evidence for solid-body rotation, and two have rotation curves that appear to be dominated by normal flat behavior.

Since all of the galaxies in this sample have probably interacted with another galaxy at some point in their history (see Table 1), the presence of noncircular motions is not surprising. Contrary to "normal" systems, however, the presence of an inner bar is not necessarily implied in these galaxies. The observed dynamics probably reflect the age and/or the strength of the interaction in most cases. For example, old mergers will be dynamically relaxed, and very weakly interacting systems will exhibit minimal perturbations. Galaxies in the advanced stages of a merger and galaxies participating in very weak interactions should therefore display relatively normal behavior. UGC 5101 is thought to be a postmerger (see, e.g., Majewski et al. 1993). This system does in fact exhibit normal dynamical behavior. In contrast, the mass distribution of intermediate-age mergers will not be relaxed. Those merging systems characterized by noncircular gas motions (e.g., UGC 8387) therefore probably correspond to intermediate age interactions. Finally, galaxies involved in strong, young interactions may be in the process of accreting gas from companion objects. This situation can manifest itself in a mass density that falls off less rapidly than that of normal galaxies. Therefore, galaxies exhibiting a solid-body rotation curve may correspond to strong, young interactions. Alternatively, some of the solid-body behavior may be an artifact caused by high optical depths. Rotation curves at longer wavelengths, although difficult to obtain, would provide additional insights regarding the dynamics of these starbursts. Such observations could potentially reveal additional noncircular motions as in the case of NGC 2146 (Prada et al. 1994) or "normal" behavior.

TABLE 11

DYNAMICAL BEHAVIOR

Galaxy	Comments	Interaction Type
UGC 4509	Weak inner bar?	Intermediate
UGC 4756B	Normal	Weak or old
UGC 5101	Normal	Weak or old
UGC 8335E	Gas from U8335W?	Intermediate
UGC 8335W.....	Inner bar	Intermediate
UGC 8387	Weak inner bar?	Intermediate
UGC 9618N	Solid body	Young
UGC 9913	Weak inner bar?	Intermediate
UGC 10647	Solid body	Young

The available data are sufficient to show that *luminous starbursts occur in a variety of interacting environments ranging from dynamically relaxed to strongly perturbed systems.* The observed dynamics provide support for the hypothesis that the recent accretion of gas or the strong noncircular motions produced by a strong interaction are responsible for many of the observed starbursts. The fact that starbursts also occur in galaxies with apparently stabilized mass distributions indicates that *enhanced star formation can continue for a lengthy period of time after an interaction event or can be triggered by relatively weak interactions.*

4. CORRELATIONS AND THE NATURE OF STAR FORMATION

The galaxies in this sample all exhibit extreme levels of star formation activity presumably triggered by an interaction or a merger with another galaxy. To understand the nature of this star formation better, we have tested our data for correlations between several observable properties: (1) the near–infrared colors measured in a 2.4 kpc aperture centered on the galaxy nucleus, (2) the K-band luminosity observed in the 2.4 kpc nuclear aperture, (3) the difference in the colors measured in the 2.4 kpc nuclear aperture and in a surrounding annulus, (4) the 5 GHz luminosity, (5) the far-infrared luminosity, (6) the [N II]/Hα line ratio, and (7) the distance between the interacting nuclei (D_{sep}), as defined in § 4.1. To determine whether two quantities are correlated, their correlation coefficient and the probability P that a random distribution could produce the correlation are evaluated. The two galaxies thought to contain AGNs (UGC 5101 and UGC 12332) are omitted from the analysis. The results are summarized in Table 12. We note that correlations were not derived for the number of ionizing photons, the total stellar OB luminosity, the infrared excess, α, or N_0 since these quantities are dependent functions of the 5 GHz and/or far-infrared luminosities.

Below, § 4.1 describes the observables chosen for the correlation analysis and discusses the definition of D_{sep}. Sections 4.2 and 4.3 discuss the quantities that appear to be correlated ($P < 1\%$): the near-infrared colors measured within a 2.4 kpc aperture centered on each galaxy component, the K-band luminosity observed within that aperture, and the far-infrared luminosity, and the difference in the colors of the 2.4 kpc aperture and an annulus surround-

TABLE 12

OBSERVED CORRELATIONS

	$J-H$	δ_{H-K}[a]	δ_{J-H}[a]	D_{sep}[b]	L_K[c]	$L_{4.85}$[c]	L_{IR}[c]	[N II]/Hα
$H-K$.....	0.71	0.59	0.57	−0.16	0.75	0.57	0.70	0.48
	(0.02)	(0.35)	(0.53)	(50)	(0.01)	(2.1)	(0.27)	(24)
$J-H$		0.47	0.73	0.00	0.72	0.14	0.31	0.72
		(2.8)	(0.01)	(100)	(0.02)	(62)	(25)	(5.0)
δ_{H-K}.....			0.81	−0.25	0.36	0.50	0.70	0.69
			(0.00)	(28)	(10)	(5.0)	(0.27)	(6.1)
δ_{J-H}				−0.06	0.48	0.29	0.55	0.80
				(79)	(2.3)	(27)	(2.8)	(1.8)
D_{sep}					0.18	−0.06	−0.02	−0.27
					(46)	(83)	(94)	(56)
L_K.....						0.46	0.59	0.52
						(7.3)	(1.7)	(20)
$L_{4.85}$.....							0.92	0.42
							(0.00)	(32)
L_{IR}								0.68
								(7.1)

NOTE.—Correlation coefficients are given for each pair of observables. The probability that the observed correlation is due to a random distribution is given as a percentage in parentheses. UGC 5101 and UGC 12332 have been omitted from the analysis.

[a] Difference between color measured within the central 2.4 kpc and a surrounding annulus.

[b] log of the distance between nuclei.

[c] log of the K, 4.85 GHz and FIR luminosities.

ing that aperture. Finally, § 4.4 discusses the behavior of the galaxies as a function of D_{sep}.

4.1. *Observables*

For the purpose of the correlation analysis, we have selected observables that can be measured on a common physical scale in order to minimize distance effects. The smallest aperture size for which near-infrared properties can be measured with confidence for the most distant galaxy in the sample is 2.″5, or 2.4 kpc. Near-infrared colors and K-band luminosities were therefore measured in the 2.4 kpc diameter aperture. For comparison, near-infrared colors were also measured in an annulus centered upon the nucleus; the inner and outer diameters of the annulus were 2.4 and 4.8 kpc, respectively. The size of the 2.4 kpc aperture on the sky, the colors and luminosities measured within that aperture, and the difference between the nuclear and annular colors are listed in Table 13. We find average near-infrared colors of $H-K = 0.53 \pm 0.15$ and $J-H = 0.80 \pm 0.15$ mag in the central 2.4 kpc, $H-K = 0.38 \pm 0.14$ and $J-H = 0.68 \pm 0.11$ mag in the surrounding annulus, and an average K-band luminosity of $(1.71 \pm 1.26) \times 10^{29}$ ergs s^{-1} Hz^{-1} in the central 2.4 kpc. CO indices are not quoted since the spectra do not possess sufficient signal-to-noise ratio to measure the emission in apertures larger than 2.″5. We note that a 2.4 kpc aperture will integrate a large fraction, if not all, of the emission from the starburst. In M82, for example, the size of the far-infrared emitting region is $\sim$0.5 kpc, and the length of the nuclear bar is $\sim$1 kpc (Telesco et al. 1991). This suggests that most of the observed far-infrared and radio emission from the 20 luminous starbursts arises from the area covered by our 2.4 kpc aperture.

As stated previously, one goal of this project is to trace the evolution of star formation in interacting systems. If the current level of star formation is related to the status of an interaction, we would expect to see correlations between the observed starburst properties and the separation of the interacting galaxy nuclei. Presumably, interacting galaxies will experience the most intense disturbances and episodes of star formation as their nuclei merge or reach their minimum separation.

To trace the evolution of star formation, we therefore assign each galaxy to an interaction class on the basis of the separation of the interacting nuclei (D_{sep}). The distances between the interacting nuclei (D_{sep}), as quoted in Table 14, refer to projected distances measured from (1) the H-band images presented in Paper II, (2) high-resolution images in the literature, or (3) optical or radio coordinates of the galaxy nuclei. An upper limit, defined as the spatial resolution of the images, is given if the parent nuclei of a galaxy merger are unresolved. A projected distance is quoted instead of the true three-dimensional separation since the observed velocity differences between interacting nuclei may be associated with either the orbital velocity of the companion or deviations in the Hubble flow. Galaxies with $D_{sep} \leq 1$ kpc are classified as Class 1 interactions. Class 1 contains galaxies whose parent nuclei appear to have merged or are currently in the process of merging. These systems are characterized by a highly disturbed morphology and strong tidal tails. Class 2 interactions consist of systems whose nuclei are separated by 1–20 kpc. Although the morphologies of the Class 2 objects are certainly not "normal," these objects generally do not possess the strong tidal features seen in other systems. Three of the members of this class contain several closely spaced (in projection) components. Finally, those galaxies possessing a dynamical companion at an effective distance in excess of 20 kpc are assigned to Class 3. The systems in Class 3 show some degree of morphological disturbance and may or may not have strong tidal features. If our hypothesis is correct, the Class 3 galaxies should be the most "normal" systems since their nuclei are the most widely separated. The Class 1 systems would show the most extreme conditions, and the Class 2 galaxies would represent intermediate stages of activity.

4.2. *Luminosities and Near-Infrared Colors*

As shown in Figures 11 and 12, the near-infrared colors measured within a 2.4 kpc aperture are correlated with the

TABLE 13

STARBURST PROPERTIES WITHIN THE CENTRAL 2.4 kpc

Galaxy	Aperture (arcsec)	$H-K$ (mag)	$J-H$ (mag)	σ_{H-K} (mag)	σ_{J-H} (mag)	log L_K[a] (ergs s^{-1} Hz^{-1})	$\delta(H-K)$[b] (mag)	$\delta(J-H)$[c] (mag)
1315	3.83	0.44	0.74	0.08	0.06	29.32	0.01	0.07
1655	6.91	0.50	0.77	0.10	0.06	29.40	0.05	0.04
2238	5.73	0.66	1.04	0.08	0.06	29.25	0.17	0.20
2608	5.27	0.41	0.75	0.08	0.08	29.24	0.11	0.11
3334[d]	9.44	0.32	0.83	0.01	0.01	28.78	...	...
3351	7.74	0.57	1.06	0.08	0.08	29.26	0.09	0.15
4509	6.74	0.57	0.83	0.04	0.04	29.17	0.35	0.25
4756A	2.51	0.51	0.71	0.06	0.04	29.18	0.16	0.01
4756B	2.51	0.55	0.72	0.06	0.04	29.07	0.13	0.05
4756C	2.51	0.38	0.64	0.06	0.06	28.74	0.22	0.10
5101[e]	3.10	0.93	0.98	0.08	0.06	29.53	0.14	0.11
6471	11.92	0.50	0.80	0.06	0.08	29.00	0.22	0.16
6472B	11.92	0.53	0.75	0.06	0.08	29.08	0.00	0.10
6472C	11.92	0.48	0.56	0.06	0.08	28.86	−0.10	−0.25
8335E	3.93	0.63	0.82	0.04	0.04	29.31	0.36	0.23
8335W	3.93	0.55	0.79	0.04	0.04	29.01	0.21	0.17
8387	5.39	0.67	0.84	0.06	0.06	29.16	0.35	0.25
8696	3.33	0.70	0.86	0.06	0.06	29.49	0.32	0.17
9618N.....	3.77	0.67	0.98	0.06	0.06	29.43	0.10	0.15
9913	6.80	0.59	1.00	0.06	0.06	29.23	0.37	0.29
10182A.....	8.25	0.23	0.54	0.06	0.06	28.54	−0.06	0.00
10182B.....	8.25	0.27	0.55	0.06	0.06	28.37	0.03	0.00
10182C.....	8.25	0.40	0.55	0.06	0.06	28.19	0.10	0.01
10647.....	6.62	0.51	0.92	0.06	0.04	29.14	0.09	0.15
12332[e].....	7.65	0.71	0.84	0.08	0.06	29.79	0.36	0.18
12815.....	8.73	0.50	0.81	0.10	0.06	29.31	0.15	0.11
M82[f]	138	0.45	0.96	0.04	0.04	28.87	...	...

NOTE.—All colors have been redshift-corrected and transformed to the CIT photometric system.

[a] Observed K-band luminosity; no extinction corrections.

[b] $(H-K)_{\rm nucleus}-(H-K)_{\rm annulus}$, where $(H-K)_{\rm nucleus}$ is the color measured in the central 2.4 kpc, and $(H-K)_{\rm annulus}$ is the color measured in an annular aperture with inner and outer diameters of 2.4 and 4.8 kpc, respectively.

[c] $(J-H)_{\rm nucleus}-(J-H)_{\rm annulus}$

[d] Data given by Bushouse & Stanford 1992 for a 5″.4 (1.4 kpc) aperture.

[e] Data are omitted from the correlation analysis (Table 12) owing to the presence of an AGN.

[f] Derived from fluxes quoted by Aaronson 1977 for a 105″ (1.8 kpc) aperture.

far-infrared and the near-infrared luminosities of the starbursts. First, the $H-K$ color increases as the far-infrared luminosity increases. The probability that this relationship could arise from a random distribution is $<1\%$. We note that the lack of a statistically significant correlation between the $J-H$ color and the far-infrared luminosity probably results from the high levels of extinction that are present in these systems. In addition, the $H-K$ and $J-H$ colors measured within a 2.4 kpc aperture increase as the K-band luminosity observed within that aperture increases. For both colors, the probability that a random distribution could produce the observed data is less than 0.02%. The similarity between the luminosities of the Class 1 and the Class 3 galaxies will be discussed in § 4.4.

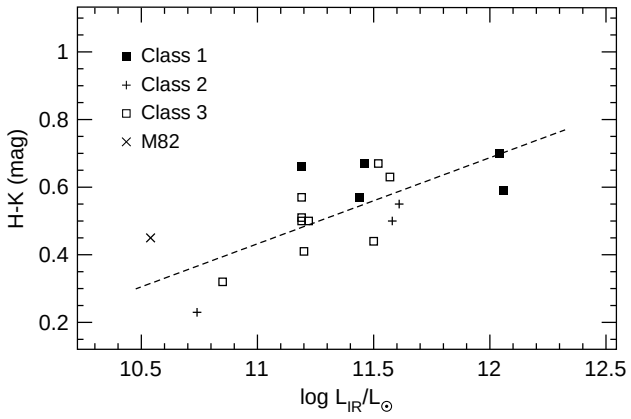

FIG. 11.—$H-K$ color and far-infrared luminosity. The correlation between the $H-K$ color and the far-infrared luminosity is displayed above. The most active starbursts possess higher quantities of obscuring and emitting dust and thus show redder colors. Those galaxies whose nuclei are separated by less than 1 kpc ("Class 1"), and those galaxies whose nuclei are separated by more than 20 kpc ("Class 3") exhibit similar luminosities (see § 4.4).

In the context of pure star formation activity, far-infrared emission arises as the light produced by the young stellar population is absorbed by dust and reradiated in the far-infrared. The reddening of the $H-K$ color with increasing far-infrared luminosity therefore suggests that this color is linked to the current level of star formation activity. In this case, the well-known radio–far-infrared correlation implies that the $H-K$ color should also be correlated with the 5 GHz luminosity. Our data indicate that the $H-K$ color tends to become redder as the radio luminosity increases; however, the correlation is not strong (see Table 12). The $H-K$ color thus appears to be more directly associated with an aspect of the far-infrared emission mechanism that is less strongly tied to the radio emission mechanism, such as the dust content of the starburst.

This scenario is complicated by the facts that AGNs tend to be more common in high-luminosity galaxies such as those included in this sample and that the presence of a

TABLE 14

INTERACTION STATUS

Galaxy	Companion[a]	D_{sep}^{b} (kpc)	Position Reference[c]	Class [d]
UGC 1315	IC 1742	1058	1	3
UGC 1655	...	...	...	3
UGC 2238	M	<0.92	2	1
UGC 2608	...	...	...	3
UGC 3334	UGC 3334a[e]	216	3	3
UGC 3351	UGC 3350	136	1	3
UGC 3608	MN	4.3	2	2
UGC 4509	M	<0.09	4	1
UGC 4756	MN	7.9	2	2
UGC 5101	M	<0.19	4	1
UGC 6471	UGC 6472	4.2	2	2
UGC 8335	MN	22	2	3
UGC 8387	M	0.30	4	1
UGC 8696	M	0.80	5	1
UGC 9618	MN	23	2	3
UGC 9913	M	0.35	6	1
UGC 10182.....	MN	1.6	2	2
UGC 10647.....	NGC 6285	36	1	3
UGC 12332.....	IC 5283	25	1	3
UGC 12815.....	UGC 12813	17	1	3
	UGC 12808	92	1	3
M82	M81	39	1	3

[a] M = merger; MN = multiple nuclei associated with the UGC source.
[b] Separation of the interacting nuclei, as projected on the sky.
[c] 1 = positions from the AGC or the NASA/IPAC Extragalactic Database (NED); 2 = H-band images; 3 = Zaritsky et al. 1993; 4 = Condon et al. 1991c; 5 = Majewski et al. 1993; 6 = Graham et al. 1990.
[d] Interaction class: 1 = $D_{sep} < 1$ kpc; 2 = $1 < D_{sep} < 20$ kpc; 3 = $D_{sep} > 20$ kpc.
[e] Closest satellite galaxy (Zaritsky et al. 1993).

low-luminosity AGN cannot be ruled out in several of the galaxies (see §§ 2.3 and 2.5). If AGNs are present in the higher luminosity galaxies, the observed correlation may simply reflect the presence or absence of an AGN. The fact that the $H-K$ color is less strongly related to the 5 GHz luminosity than the far-infrared luminosity would not be surprising in this case since the radio and the far-infrared luminosities of AGNs do not exhibit the strong correlation seen in star-forming galaxies (CFB91, and references therein). The existence of red, luminous starbursts that lack convincing evidence of an AGN (e.g., UGC 8387 and UGC 8335) and relatively blue starbursts that exhibit evidence of Seyfert activity (e.g., UGC 2608) pose a problem for this interpretation of the data, however. This difficulty can be resolved if the correlation between the $H-K$ color and the far-infrared luminosity for galaxies harboring both a low-luminosity AGN and an intense starburst is interpreted in terms of the dust content of the system. In this scenario, redder, higher luminosity systems have more obscuring and emitting dust than bluer, lower luminosity systems.

We conclude that the observed correlation implies that the $H-K$ color traces the *amounts of obscuring and emitting dust associated with the nuclear region*, whether the nucleus contains a pure starburst or a starburst accompanied by an AGN. The observed correlation between the K-band luminosity and the $H-K$ and $J-H$ colors suggests that the mechanism associated with the reddening of the emission is also linked to increases in the observed luminosity. Finally, the data imply that the near-infrared colors also serve as an indirect measure of *the violence of the nuclear activity*, whether it be a "pure" starburst or a starburst accompanied by a low-luminosity AGN, since the luminosity of a system can be considered a measure of its activity level.

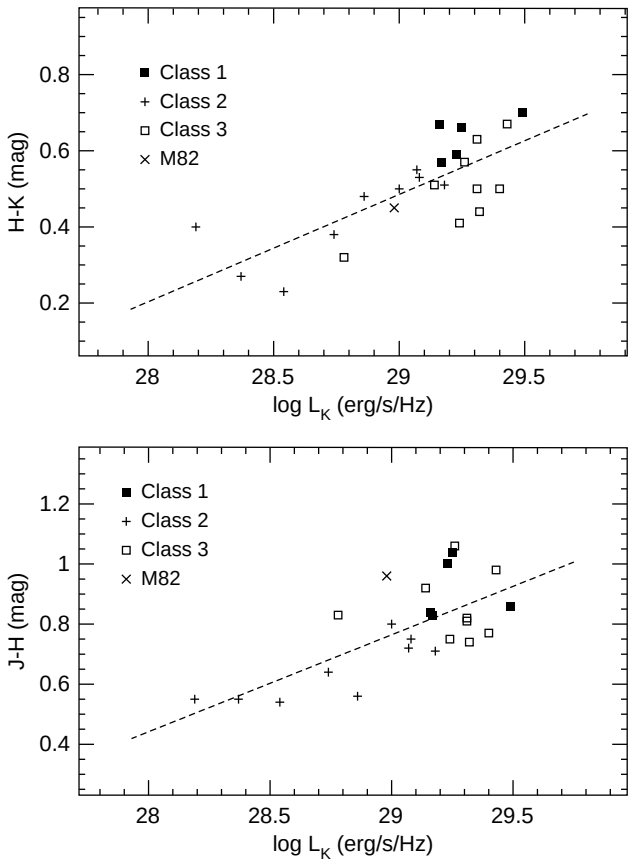

FIG. 12.—Near-infrared colors and the K-band luminosity. The relationships between the $H-K$ and $J-H$ colors and the K-band luminosity observed within the central 2.4 kpc are illustrated above. The correlation between the colors and the K-band luminosity implies the mechanism responsible for the enhanced luminosity is also associated with the red colors observed in starburst nuclei. Emission from obscured red and blue stars and from hot dust will produce both red colors and an increase in the observed luminosity. Mergers ("Class 1" systems) and widely separated nuclei ("Class 3" systems) display similar K-band luminosities (see § 4.4).

The observed relationships can be understood in terms of the interplay among the stellar, dust, and gaseous components of a starburst that naturally results from the large amounts of gas and dust channeled to the nuclear regions of interacting galaxies. The galaxies with higher far-infrared luminosities are presumably undergoing more intense star formation and will therefore contain larger numbers of young stars, as well as larger amounts of dust and molecular material. The numerous young hot stars will act as both a luminosity source and a potential heating source for the dust. As intermediate-mass stars evolve off the main sequence and reach the red supergiant stage, they will produce a dramatic increase in the K-band luminosity. An AGN, if present, will function as an additional heating and luminosity source. If the dust is heated to sufficiently high temperatures by either young stars or an AGN, the emission from the hot dust will also increase the K-band luminosity and redden the colors of the starburst (see also § 2.3). Finally, the large amounts of dust and gas will obscure and consequently redden the stellar and nonstellar emission produced by the starburst (and AGN). The observed colors and luminosities are consistent with this "standard" starburst/AGN scenario.

4.3. *The Spatial Extent of Star Formation*

Since the near-infrared colors appear to be linked to the central luminosity, they also provide an indirect measure of the strength of the nuclear star formation activity and any accompanying AGN activity. A comparison between the colors measured on and off the nucleus of the starburst galaxy therefore yields information regarding the spatial properties of the activity. In § 3.1, we found that the star formation in these systems is spatially extended. Figure 13 shows that the difference in the colors observed in the nucleus and in a surrounding annulus increases as the $H-K$ color reddens. This correlation implies that the activity in the reddest galaxies is more *strongly peaked*. Red starbursts that are not accompanied by an AGN are then characterized by a strong core of star formation activity. In cases in which an AGN is also present, the spatial peaking of the activity may simply reflect the presence of the AGN.

The galaxies with the reddest nuclear $J-H$ colors also have the reddest annular $J-H$ colors (Fig. 14). The probability that this correlation could be produced by a random distribution is $<1\%$. The reddest nuclear $H-K$ colors tend to correspond to the reddest annular $H-K$ colors, although the scatter in this relationship is larger than in the case of the $J-H$ colors. The increased scatter could indicate that the nuclear and the annular $H-K$ colors are sometimes influenced by different processes, e.g., emission

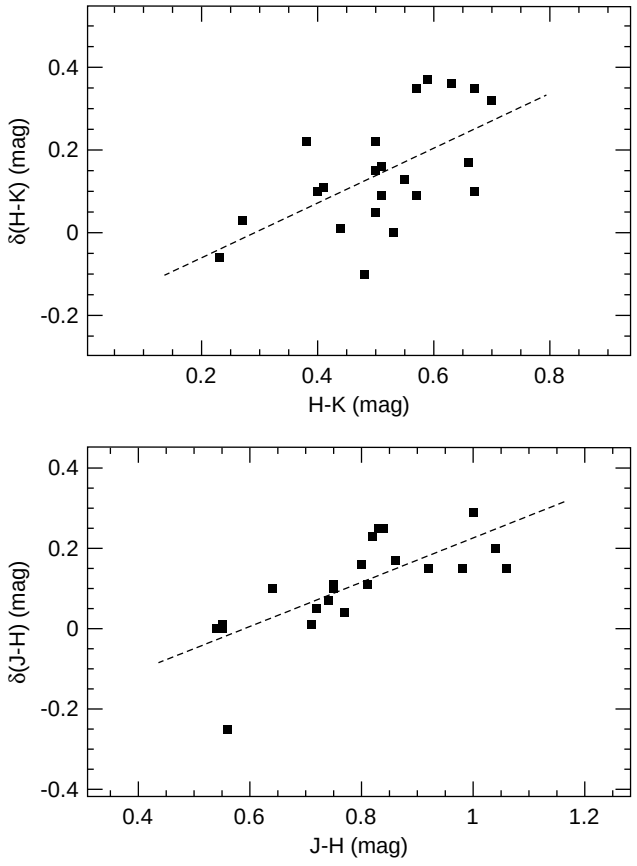

FIG. 13.—Change in the near-infrared colors. This figure shows the relationship between the nuclear colors and the change in the colors between the central 2.4 kpc and a surrounding annulus (inner diameter = 2.4 kpc; outer diameter = 4.8 kpc). The reddest nuclei exhibit the largest change in colors, which implies that the most active galaxies are characterized by strong central peaks of star formation and possibly AGN activity.

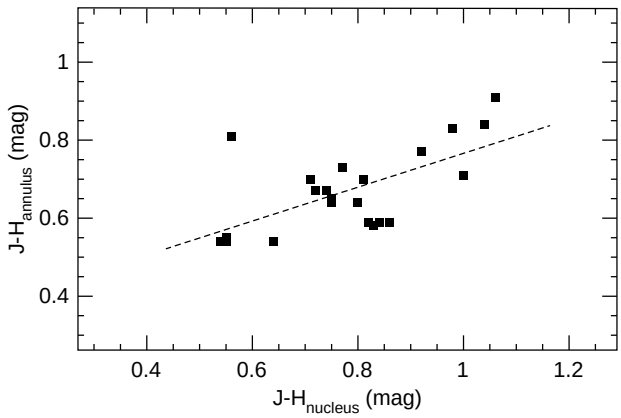

FIG. 14.—Nuclear and off-nuclear near-infrared colors. The correlations between the colors measured within the central 2.4 kpc and within a surrounding annulus (inner diameter = 2.4 kpc; outer diameter = 4.8 kpc) are illustrated above. The fact that the reddest nuclei exhibit the reddest annuli suggests that violent star formation activity is present over larger spatial extents in the most active systems.

from hot dust heated by star formation and/or AGN activity. Since the reddest galaxies are the most luminous and hence the most active, the relationship between the nuclear and the annular colors suggests that the *physical extent of violent star formation activity is larger* in the redder galaxies. The hot young stars should therefore be distributed over a larger region. For those galaxies with high-resolution radio maps, a correlation between the size of the radio-emitting region and the $H-K$ color is present. We conclude that the reddest galaxies show the largest enhancements in both the core and disk star formation activity; the activity levels of the cores increase faster than those of the disks.

These correlations hold implications for both the fueling and the propagation of the starbursts. First, the central peaking of the star formation in the reddest galaxies suggests that large amounts of fuel for star formation activity, and possibly AGN activity, are concentrated within a small area. This situation may reflect a highly efficient funneling of gas into the nucleus. The increase in the spatial extent of the star formation is probably related to several factors, including the intensity and the age of the burst, as well as the mechanism fueling the burst. For example, older, more intense bursts may have propagated further into the disk of the host galaxy. Star formation may also be triggered in the disk of a galaxy as gas flows into the nucleus.

4.4. *The Distance between the Galaxy Nuclei*

As discussed in § 4.1, correlations between the star formation properties and the separation of the interacting galaxy nuclei may trace the evolution of starburst activity. Figures 11, 12, and 15 illustrate the near-infrared behavior of each of the three classes as a test of this hypothesis. In Figure 15, we see that the near-infrared colors of the Class 1 and Class 3 interactions are quite similar. The colors of the Class 2 interaction galaxies tend to be bluer than those of the other galaxies. The luminosities of the Class 1 and Class 3 galaxies show similar behavior, as illustrated in Figures 11 and 12. We note that the luminosity behavior in Figure 11 could represent a selection effect. The far-infrared luminosities reflect the total luminosities of each interacting system since they are derived from wide-beam measurements. By selecting the most luminous systems, we expect to select prefer-

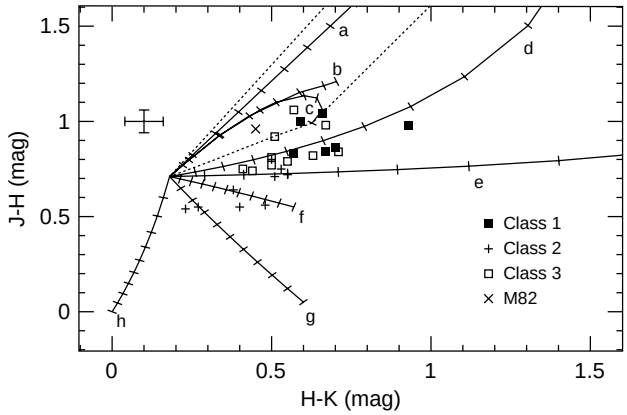

FIG. 15.—Colors observed within a 2.4 kpc aperture. The colors measured within a 2.4 kpc aperture centered on each galaxy nucleus are displayed with representative uncertainties. For comparison, the colors of evolved stars, mixing curves, and extinction vectors are also shown as in Fig. 3. The "Class 1" ($D_{sep} < 1$ kpc) and "Class 3" ($D_{sep} > 20$ kpc) systems are characterized by similar colors.

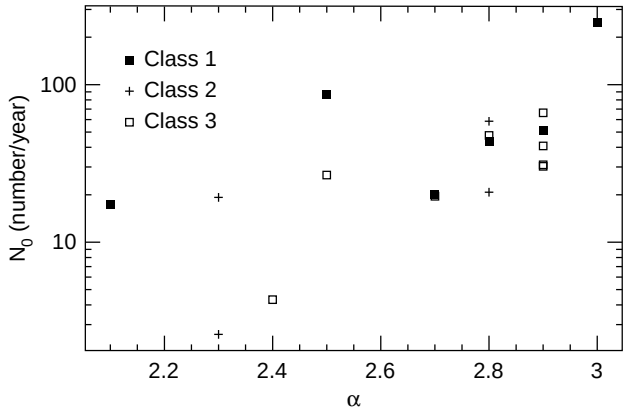

FIG. 16.—IMF parameters. The normalization constant (N_0) and slope (α) of the IMF are displayed for each of the three interaction classes discussed in the text. No relationship exists between the star formation rate, the IMF slope, and the distance between the galaxy nuclei. The "intensity" of the burst may be regulated by other parameters such as the internal structures of the galaxies.

entially interacting systems in which both members are luminous. One then expects that the luminosity of the starbursting component may be significantly less than the total system luminosity. However, high-resolution radio mapping (Condon et al. 1990) indicates that generally 80%–90% of the radio and the far-infrared emission associated with the Class 3 systems arises solely from the starbursting member of the system. This issue does not apply to the K-band luminosities since these are derived for 2.4 kpc apertures centered upon the individual starbursting components.

The observed color and luminosity behavior of the Class 3 galaxies is somewhat puzzling and suggests several possibilities regarding the evolution of star formation. If the interacting nuclei have not yet reached the point of closest approach, or are currently at the point of closest approach, the fact that their near-infrared luminosities and colors are similar to those of merging systems suggests that the strength of the burst is not determined by the level of contact between the interacting nuclei. Although the burst is triggered by the interaction, the intensity may be more strongly regulated by the internal structure of the interacting galaxies than their nuclear separations (Mihos & Hernquist 1994). This hypothesis is also consistent with the lack of a relationship between the values of α and N_0 of the galaxies, as illustrated in Figure 16.

If the Class 3 systems have already passed the point of closest approach, the interactions must be $\sim 10^8$–10^9 yr old to allow sufficient time for the galaxies to reach their current separations. Assuming the observed starbursts were triggered prior to or during the point of closest approach, the properties of the Class 3 galaxies imply that the duration of intense starburst activity may be as long as 10^9 yr. The interaction must resupply the starburst nucleus with gas in order to maintain the observed star formation rates over this extended period of time. Alternatively, we may be witnessing a significant time delay between the maximum disturbance within a galaxy and the onset of star formation.

Finally, the starbursts occurring in the Class 3 systems may have been triggered by the accretion of a small satellite, as opposed to an interaction with the optical companion. A merger with even a low-mass, gas-poor system can trigger nuclear activity (Majewski et al. 1993). In this case, the Class 3 galaxies are really postmergers, and similarities with the Class 1 galaxies should be expected.

5. CONCLUSIONS

We have selected the 20 UGC starburst galaxies with the highest radio luminosities from Condon et al. (1991b) for a multiwavelength analysis of the starburst phenomenon. These galaxies form a sample of relatively nearby northern hemisphere starbursts that is independent of the dust content and the morphology of the host galaxy. For this sample of starburst galaxies, we conclude the following:

1. The intrinsic ionizing fluxes produced by these starbursts are significantly higher than that produced by M82. The average ionizing flux is $N_{UV} = (1.13 \pm 1.18) \times 10^{55}$ s^{-1}.

2. With an average nominal value of IRE $= 7.5 \pm 2.4$, the infrared excesses of these starbursts are lower than and span a narrower range of values than the infrared excesses of Galactic H II regions. The IRE of M82 is also lower than the values typical of Galactic H II regions. The data suggest that the absorption of nonionizing emission from low-mass stars may play a smaller role in powering the far-infrared emission in starburst systems than in Galactic H II regions. This situation can result from an IMF that favors the creation of high-mass stars. Alternatively, the starbursts may simply contain fewer old H II regions than the Milky Way. The starburst IREs are also likely to be influenced by the presence of large amounts of gas that enable the starburst H II regions to absorb a larger fraction of the Lyman continuum photons than Galactic H II regions.

3. The average value of the ratio of the OB stellar and the far-infrared luminosities derived from radio fluxes and a Miller & Scalo IMF is $L_{OB}/L_{IR} = 3.58 \pm 1.25$. The fact that this quantity exceeds unity suggests that a Miller & Scalo IMF overestimates the stellar luminosity in the radio-luminous starbursts. An IMF slope of 2.7 ± 0.2 is more appropriate for the mass range $M > 10\ M_\odot$. The upper mass range of the starburst IMF thus bears a strong similarity to that of Magellanic OB associations.

4. The central 2.″5 of the radio-luminous starbursts is characterized by average near-infrared colors of

$H-K = 0.64 \pm 0.25$ and $J-H = 0.87 \pm 0.18$ mag. The starbursts are generally redder than less luminous starbursts studied previously in the literature and are similar in color to infrared-bright galaxies.

Assuming that a Galactic or SMC extinction law can be applied to the starbursts and that the starbursts are characterized by a known reddening curve, the nuclear near-infrared colors of the majority of the starbursts cannot be explained solely in terms of an obscured mixture of red giants and red supergiants. The colors of many of the starbursts can be explained by heavily obscured emission from red stars, with small contributions to the K-band flux from blue stars ($\approx 10\%$), thermal gas ($\approx 5\%$), and hot dust ($\approx 5\%$). Some of the starbursts are characterized by colors that are too extreme to be explained by this scenario. These systems require a larger contribution from blue stars, and in some cases, from hot dust. Some of the colors may also reflect the presence of a low-luminosity AGN accompanying the starburst. In cases in which dust emission is present, a new result is that the level of dust emission is higher than that expected from observations of Galactic H II regions. We note that the utility of $H-K$ versus $J-H$ color plots as an extinction diagnostic is reduced because of the presence of emission from blue stars and possibly hot dust, as well as the fact that the geometry of the obscuring dust is not known.

Correlations between the $H-K$ color and the far-infrared and the near-infrared luminosities indicate that the $H-K$ color traces the dust content of these galaxies and that the mechanism associated with the reddening of the near-infrared emission is also associated with an increase in the near-infrared luminosity. The near-infrared colors provide an indirect measure of the relative strength of the nuclear activity, whether it be a "pure" starburst, or a starburst accompanied by a low-luminosity AGN.

5. The star formation activity occurring in an annular aperture with inner and outer diameters of 2.4 and 4.8 kpc is characterized by average near-infrared colors of $H-K = 0.38 \pm 0.14$ and $J-H = 0.68 \pm 0.11$ mag. The near-infrared colors of the central 2.4 kpc are $H-K = 0.53 \pm 0.15$ and $J-H = 0.80 \pm 0.15$. Together, the off-nuclear near-infrared colors and published radio data indicate that the starburst activity is extended. That is, the 20 CFB91 starbursts are not strictly nuclear starbursts, in contrast to the starbursts studied by Balzano (1983) and Devereux (1989).

The fact that the reddest galaxies exhibit the largest difference between their nuclear and annular colors implies that the starburst activity in these systems is strongly peaked. In cases in which a low-luminosity AGN accompanies the starburst, the strong peak in the colors may simply reflect the presence of the AGN. Violent star formation also appears to be present over a larger physical scale in these systems since the galaxies with the reddest nuclear colors also possess the reddest annular colors.

6. The starbursts possess an average photometric CO index of 0.14 ± 0.04 mag. While several of the starburst nuclei are characterized by CO indices that are similar to those of E/S0 galaxies, the observed CO indices span a wider range of values than those of E/S0 galaxies. The observed CO indices represent lower limits to the intrinsic values; many of the CO indices appear to be diluted by emission from blue stars and possibly hot dust. Consequently, the value of the CO index does not always immediately rule out or confirm the presence of young red supergiants.

7. For the 16 starbursts with measured optical line ratios, six have nuclear line ratios consistent with pure star formation activity, seven exhibit LINER activity, and three show evidence of Seyfert activity. The nuclear line ratios are strongly correlated with those observed off the nucleus. The presence of spatially extended LINER emission suggests that the line ratios are produced by shocks resulting from superwinds and/or violent galaxy-galaxy interactions and mergers, rather than by a low-luminosity AGN. Similar effects have been observed in infrared luminous galaxies (Veilleux et al. 1995).

8. The 20 starbursts were presumably triggered by galaxy-galaxy interactions and mergers. We find that radio-luminous starbursts can occur in a variety of environments, ranging from dynamically relaxed to strongly perturbed systems.

9. Starbursts occurring in merging systems and systems with widely separated nuclei are characterized by similar colors and luminosities. This fact suggests three possibilities: (1) the intensity of a burst may be determined by the internal structures of the interacting galaxies instead of their nuclear separations; (2) a time delay may occur between the point of closest approach and the onset of star formation; and/or (3) the widely separated systems may actually be postmergers between the galaxy hosting the starburst and a dwarf companion.

We wish to thank an anonymous referee for a timely and insightful review of our paper. We also wish to thank Karl Gordon for providing the majority of the reddening models used in this paper and for many discussions regarding extinction in starbursts. D. A. S. acknowledges support from the NASA Graduate Student Researchers Program. This research is also supported by NSF grants AST 95-28860 to M. P. H. and T. H. and AST 90-23450 to M. P. H. During the final stages of manuscript preparation, additional financial support for D. A. S. was provided by a National Research Council–GSFC Research Associateship and by NASA grant NAG 5-1630 to the FOS science team. This research has made use of the NASA/IPAC Extragalactic Database (NED) which is operated by the Jet Propulsion Laboratory, Caltech, under contract with the National Aeronautics and Space Administration.

REFERENCES

Aaronson, M. 1977, Ph.D. thesis, Harvard Univ.
Arendt, R. G., et al. 1994, ApJ, 425, L85
Armus, L., Heckman, T. M., & Miley, G. K. 1989, ApJ, 347, 727
Ashby, M. L. N., Houck, J. R., & Matthews, K. 1995, ApJ, 447, 545
Baldwin, J. A., Phillips, M. M., & Terlevich, R. 1981, MNRAS, 93, 5
Balzano, V. A. 1983, ApJ, 268, 602
Bessel, M. S., & Brett, J. M. 1988, PASP, 100, 1134
Bosma, A., Byun, Y., Freeman, K. C., & Athanassoula, E. 1992, ApJ, 400, L21
Bushouse, H. A., & Stanford, S. A. 1992, ApJS, 79, 213
Calzetti, D. 1997, AJ, 113, 162
Calzetti, D., Bohlin, R. C., Kinney, A. L., Storchi-Bergmann, T., & Heckman, T. M. 1995, ApJ, 443, 136
Calzetti, D., Kinney, A. L., & Storchi-Bergmann, T. 1994, ApJ, 429, 582
Carico, D. P., Sanders, D. B., Soifer, B. T., Elias, J. H., Matthews, K., & Neugebauer, G. 1988, AJ, 95, 356
Cohen, J. G., Frogel, J. A., Persson, S. E., & Elias, J. H. 1981, ApJ, 249, 481
Condon, J. J. 1992, ARA&A, 30, 575
Condon, J. J., Anderson, M. L., & Helou, G. 1991a, ApJ, 376, 95
Condon, J. J., & Broderick, J. J. 1988, AJ, 101, 362

Condon, J. J., Frayer, D. T., & Broderick, J. J. 1991b, AJ, 101, 362 (CFB91)
Condon, J. J., Helou, G., Sanders, D. B., & Soifer, B. T. 1990, ApJS, 73, 359
Condon, J. J., Huang, Z.-P., Yin, Q. F., & Thuan, T. X. 1991c, ApJ, 378, 65
Condon, J. J., & Yin, Q. F. 1990, ApJ, 357, 97
Couch, W. J., Ellis, R. S., Sharples, R. M., & Smail, I. 1994, ApJ, 430, 121
Devereux, N. A. 1989, ApJ, 346, 126
Doane, J. S., & Mathews, W. G. 1993, ApJ, 419, 573
Dressler, A., Oemler, A., Butcher, H. R., & Gunn, J. E. 1994, ApJ, 430, 107
Draine, B. T. 1989, in 22nd ESLAB Symposium, Infrared Spectroscopy in Astronomy, ed. B. H. Kaldeich (Noordwijk: ESA), 93
Driver, S. P., Windhorst, R. A., & Griffiths, R. E. 1995, ApJ, 453, 48
Dudley, C. C., & Wynn-Williams, C. G. 1993, ApJ, 407, L65
Evans, I. N., & Dopita, M. A. 1985, ApJS, 58, 125
Filippenko, A. V. 1989, in Active Galactic Nuclei, ed. D. E. Osterbrock & J. S. Miller (Dordrecht: Kluwer), 495
Frogel, J. A. 1985, ApJ, 298, 528
Frogel, J. A., Persson, S. E., Aaronson, M., & Matthews, K. 1978, ApJ, 220, 75
Gehrz, R. D., Sramek, R. A., & Weedman, D. W. 1983, ApJ, 267, 551
Giovanelli, R., Haynes, M. P., & Chincarini, G. L. 1982, ApJ, 262, 442
Glass, I. S., & Moorwood, A. F. M. 1985, MNRAS, 214, 429
Goad, J. W., & Roberts, M. S. 1981, ApJ, 250, 79
Goldader, J. D., Joseph, R. D., Doyon, R., & Sanders, D. B. 1995, ApJ, 444, 97
Gordon, K. D., Calzetti, D., & Witt, A. N. 1997, ApJ, 487, 625 (GCW)
Graham, J. R., Carico, D. P., Matthews, K., Neugebauer, G., Soifer, B. T., & Wilson, T. D. 1990, ApJ, 354, L5
Heckman, T. M. 1981, ApJ, 250, L59
Heckman, T. M., Armus, L., & Miley, G. K. 1990, ApJS, 74, 833
Helou, G., Khan, I. R., Malek, L., & Boehmer, L. 1988, ApJS, 68, 151
Helou, G., Soifer, B. T., & Rowan-Robinson, M. 1985, ApJ, 298, 7
Hill, R. J., Madore, B. F., & Freedman, W. L. 1994, ApJ, 429, 204
Ho, L. C., Filippenko, A. V., & Sargent, W. L. W. 1993, ApJ, 417, 63
Ho, P. T. P., & Haschick, A. D. 1981, ApJ, 248, 622
Joseph, R. D., Meikle, W. P. S., Robertson, N. A., & Wright, G. S. 1984, MNRAS, 209, 111
Kleinmann, S. G., & Hall, D. N. B. 1986, ApJS, 62, 501
Koornneef, J. 1983, A&A, 128, 84
Landini, M., Natta, A., Oliva, E., Salinari, P., & Moorwood, A. F. M. 1984, A&A, 134, 284
Larkin, J. E., Graham, J. R., Matthews, K., Soifer, B. T., Beckwith, S., Herbst, T. M., & Quillen, A. C. 1994, ApJ, 420, 159
Larson, R. B. 1974, MNRAS, 166, 585
Lester, D. F., Carr, J. S., Joy, M., & Gaffney, N. 1990, ApJ, 352, 544
Lonsdale, C. J., Helou, G., Good, J. C., & Rice, W. L. 1985, Catalogued Galaxies and Quasars Observed in the *IRAS* Survey (Washington, D.C.: US Government Printing Office)
Lonsdale, C. J., Lonsdale, C. J., & Smith, H. E. 1995, BAAS, 187, 5008
Lonsdale, C. J., Smith, H. E., & Lonsdale, C. J. 1993, ApJ, 405, L9
Maeder, A., & Meynet, G. 1988, A&AS, 76, 411
Majewski, S. R., Hereld, M., Koo, D. C., Illingworth, G. D., & Heckman, T. M. 1993, ApJ, 402, 125
Massey, P., Lang, C. C., Degioia-Eastwood, K., & Garmany, C. D. 1995, ApJ, 438, 188
Mathis, J. S. 1990, ARA&A, 28, 37
Mazzarella, J. M., & Balzano, V. A. 1986, ApJS, 62, 751
Mazzarella, J. M., Soifer, B. T., Graham, J. R., Hafer, C. I., Neugebauer, G., & Matthews, K. 1992, AJ, 103, 413
Mazzarella, J. M., Voit, G. M., Soifer, B. T., Matthews, K., Graham, J. R., Armus, L., & Shupe, D. 1994, AJ, 107, 1274
McLeod, K. K., Rieke, G. H., Rieke, M. J., & Kelly, D. M. 1993, ApJ, 412, 111
Mihos, J. C., & Hernquist, L. 1994, ApJ, 431, L9
Myers, P. C., Dame, T. M., Thaddeus, P., Cohen, R. S., Silverberg, R. F., Dwek, E., & Hauser, M. G. 1986, ApJ, 301, 398
Panagia, N. 1973, AJ, 78, 929
———. 1974, ApJ, 192, 221
Petrosian, V., Silk, J., & Field, G. B. 1972, ApJ, 177, L69
Prada, F., Beckman, J. E., McKeith, C. D., Castles, J., & Greve, A. 1994, ApJ, 423, L35
Ridgway, S. E., Wynn-Williams, C. G., & Becklin, E. E. 1994, ApJ, 428, 609
Rieke, G. H., Lebofsky, M. J., Thompson, R. I., Low, F. J., & Tokunaga, A. T. 1980, ApJ, 238, 24
Rieke, G. H., Loken, K., Rieke, M. J., & Tamblyn, P. 1993, ApJ, 412, 99
Satyapal, S., Watson, D. M., Pipher, J. L., Forrest, W. J., Greenhouse, M. A., Smith, H. A., Fischer, J., & Woodward, C. E. 1997, ApJ, 483, 148
Scoville, N. Z., & Good, J. C. 1989, ApJ, 339, 149
Schaller, G., Schaerer, D., Meynet, G., & Maeder, A. 1992, A&AS, 96, 269
Schmidt-Kaler, Th. 1982, in Landolt-Börnstein, Vol. VI/2b, Stars and Star Clusters, ed. K. Schaifers & H. H. Voigt (Berlin: Springer), 451
Shields, J. C., & Kennicutt, R. C. 1995, ApJ, 454, 807
Smith, D. A., Herter, T., Haynes, M. P., Beichman, C. A., & Gautier, T. N. 1995, ApJ, 439, 623 (Paper I)
———. 1996, ApJS, 104, 217 (Paper II)
Soifer, B. T., Houck, J. R., & Neugebauer, G. 1987, ARA&A, 25, 187
Telesco, C. M., Campins, H., Joy, M., Dietz, K., & Decher, R. 1991, ApJ, 369, 135
Tendrup, D. M., Davies, R. L., Frogel, J. A., DePoy, D. L., & Wells, L. A. 1994, ApJ, 432, 518
Terlevich, R., & Melnick, J. 1985, MNRAS, 213, 841
Terlevich, R., Tenorio-Tagle, G., Różyczka, M., Franco, J., & Melnick, J. 1995, MNRAS, 272, 198
Turner, P. C., Forrest, W. J., Pipher, J. L., & Shure, M. A. 1992, ApJ, 393, 648
Veilleux, S., Kim, D.-C., Sanders, D. B., Mazzarella, J. M., & Soifer, B. T. 1995, ApJS, 98, 171
Veilleux, S., & Osterbrock, D. E. 1987, ApJS, 63, 295
Wang, Z., Scoville, N. Z., & Sanders, D. B. 1991, ApJ, 368, 112
Whittet, D. C. B. 1992, Dust in the Galactic Environment (Bristol: IOP)
Willner, S. P., Soifer, B. T., Russell, R. W., Joyce, R. R., & Gillett, F. C. 1977, ApJ, 217, L121
Witt, A. N., & Gordon, K. D. 1996, ApJ, 463, 681
Zaritsky, D., Smith, R., Frenk, C., & White, S. D. M. 1993, ApJ, 405, 464
Zhou, S., Wynn-Williams, C. G., & Sanders, D. B. 1993, ApJ, 409, 149